5-1-2018

Simulation and Optimal Integration of a Heat Recovery Steam Generator with Solar Thermal Energy

Tianjun Han
Lehigh University, tih216@lehigh.edu

Simulation and Optimal Integration of a Heat Recovery Steam Generator with Solar Thermal Energy

by

Tianjun Han

A Thesis

Presented to the Graduate and Research Committee

of Lehigh University

in Candidacy for the Degree of

Master of Science

in

Mechanical Engineering

Lehigh University

May 2018

This thesis is accepted and approved in partial fulfillment of the requirements for the Master of Science

_____
Date

_____
Dr. Alparslan Oztekin, Thesis Advisor

_____
Dr. Gary Harlow, Chairperson of Departmen

ACKNOWLEDGEMENTS

I would like to express my greatest gratitude to my thesis advisors, Dr. Carlos E. Romero and Dr. Alparslan Oztekin. They gave me a lot of guidance on my research whenever I had questions. Additionally, I would like to thank PhD student, Xingchao Wang, at Lehigh University. He patiently taught me how to use ASPEN Plus and make a logical organization of my thesis, which helped me a lot. I had a really great time at the ERC of Lehigh University and have obtained a lot of great memories with my friends, CJ Pan, Dr. Zongliang Qiao, Dr. You Lv and Guanrong Song.

I am also very appreciative of all the encouragement and support my parents gave me, which is the motivation that drived me forward during my graduate study. Moreover, I want to thank my friend, Huazhi Chen, for offering me a lot of company all the time. At the end, special thanks to Dr. Carlos E. Romero again for his hours of thesis guidance and proofreading.

CONTENTS

LIST OF TABLES

LIST OF FIGURES

ABSTRACT

With the increasing industrial manufacturing, commercial activities and better living conditions of world population, the consumption of electricity increases steadily. However, the world consumption of fossil fuels, which is the traditional source of electricity, is being reduced due to the impact of air pollution caused by the burning of fossil fuels.

The integration of the Combined Cycle (CC) power plant with solar energy have recently been regarded as a good choice to mitigate high consumption of fossil fuels for a better environment for the reason that solar collectors can be coupled with the steam cycle side of CC power plant which is also called a Heat Recovery Steam Generator (HRSG). In this paper, the HRSG of a CC power plant located in Mexico was studied and simulated in ASPEN Plus. Different methods of adding solar thermal energy into the CC system are presented. The concept of solar conversion rate is introduced which is the ratio of net power output increase after the solar thermal energy is integrated into the fossil part of the plant over value of solar thermal energy to quantify the performance of each method of integration. Operational constrains on temperature of the feed water leaving a solar heat exchanger and the extraction ratio of the feed water are introduced. A comparison of solar conversion rates for different methods with different values of solar input, and different flow rates of the feed water were investigated. The results show that heating the feed water leaving the HRSG's superheater and extracting the feed water leaving the evaporator while sending it back to a location after the superheater are most effective ways to achieve the largest solar conversion rate.

This paper is based on a real power plant and provides an integration on how to effect and achieve the largest solar conversion rate within reasonable limits of the practical thermal plant

operation. This provides guidance on a method to Integrated Solar Combined Cycle Power Plants (ISCC) for largest solar conversion rate.

CHAPTER 1: Introduction

Improvements in the quality of life and industrial production of developing countries together with an increase in population all over the world has led to a much greater demand for fossil fuels [1]. The reserves of fossil fuels like oil, coal and gas will keep decreasing [2]. Additionally, there are a lot of environmental issues related to the burning of fossil fuels. Dincer and Rosen [3] reported evidence that shows the damage of acid precipitation formed by sulphur dioxide (SO_2) and nitrogen oxides (NO_x) from the combustion of fossil fuels which can be transported in atmosphere and bring damage to the ecosystem. It is also generally acknowledged that the greenhouse gases have a large effect on global warming. Carbon dioxide (CO_2) released from the process of fossil fuel combustion is believed to account for 50% of global greenhouse gases [2]. Colonbo [4] has made a prediction that if the amount of greenhouse gases in the atmosphere keeps increasing at the present rate, the earth's surface temperature is expected to increase by 2-4 °C and sea levels are expected to rise by 30-60 cm. With this level of prediction, there could be flooding of coastal settlements, moving agricultural activity to lands at higher latitude and loss of access to needed fresh water.

Renewable energy technologies which convert solar energy to useful thermal and electrical energy have the potential of supplying energy with almost zero emissions of both greenhouse gases and air pollutants [1, 2]. Besides, other benefits arise after renewable energy systems are installed. Consumption of fossils fuels which are used for generating electricity would decrease. Operation of renewable energy systems can create a number of job opportunities in rural areas, which can mitigate people's migration towards urban areas [5]. However, the most important benefit is that renewable energy systems can help decrease environmental pollution, making it possible for

developing countries to fulfill international agreements on environmental protection while at the same time meeting the demand by increased big consumption of electricity [6].

Renewable energy resources, also called alternative sources of energy, includes solar energy, biomass energy, wind energy, hydraulic energy, geothermal energy [7]. Among all these forms of renewable energy sources, solar energy is always regarded as the most promising option for the reason that solar energy is the most abundant, and it nearly generates zero noise or pollution to the environment [8]. A good body of research has been done on various types of solar collectors which can be categorized into stationary collectors and sun tracking concentrating collectors [2]. Stationary collectors are permanently fixed in one position, making them unable to track the sun. Flat-plate collectors and compound parabolic collectors are two typical types of stationary collectors. A diagram of a flat-plate collector is shown in Figure. 1. In this diagram, the solar collector absorbs solar energy and transport it to the transport medium, making it able to be carried

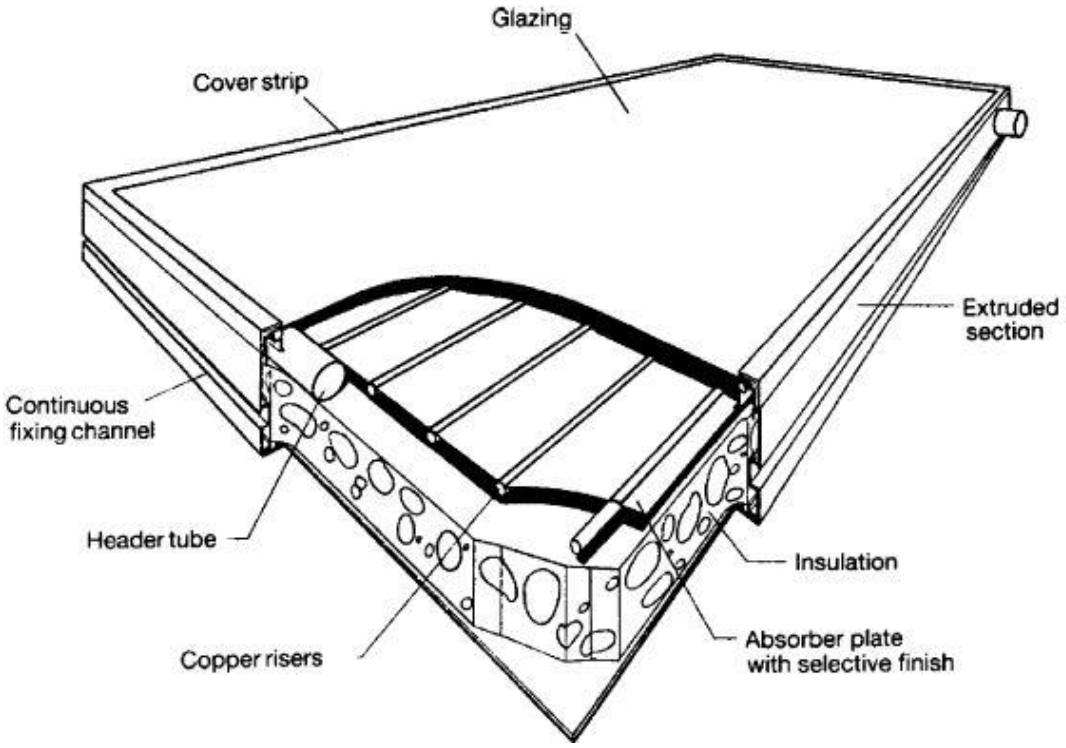

Fig. 1. Flat-plate collector [2]

away for use or storage when solar radiation passes through a transparent cover and impinges on a blackened absorber surface with high absorptivity. Compound parabolic collectors absorb solar radiation over a wide range of angles by using multiple internal reflections, so the need to move this type of solar collectors, to adjust to the change of solar orientation can be avoided. A compound parabolic collector is depicted in Figure. 2. Sun tracking concentrating collectors can

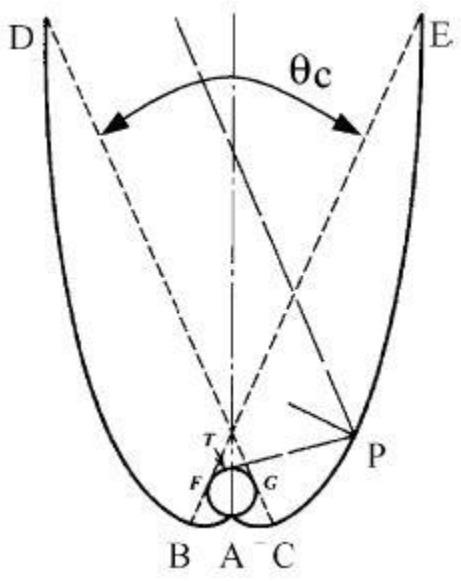

Fig. 2. Schematic diagram of the compound parabolic collector [2]

follow the movement of the sun and generate higher working temperature of the heat transfer fluid with smaller concentration area, while at the same time having smaller heat losses. The parabolic trough collector is a typical type of sun tracking concentrating collectors. Parabolic trough collectors are made by bending a piece of material with great reflectivity into a parabolic shape which can make parallel solar radiation reflect on a receiver tube, supported by a single tracking axis [2]. A schematic of the parabolic trough collector is illustrated in Figure. 3.

Solar energy have been widely used in both domestic and industrial processes. It has been proved that solar cooking can help save 16.8 million tons of fire wood and reduce emissions of 38.4 million tons of CO_2, if it is used 6-8 months per year [9]. Some textile industries also use

solar thermal energy to heat water to around 100 °C for dying, bleaching and washing [10]. Apart from heating, solar energy can also provide refrigeration for food and medicine preservation and provide comfort cooling. Solar refrigeration systems, which consist of evaporation and absorption cycles, have saved companies significant resources by reducing consumption of electricity in many applications [2], (see Figure. 4).

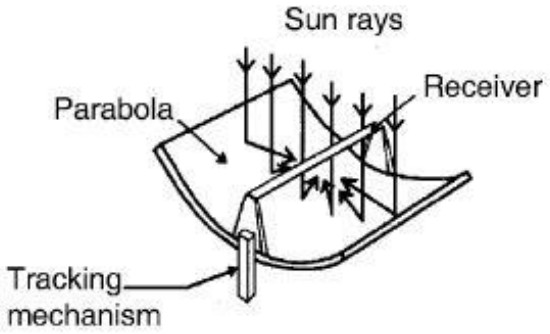

Fig. 3. Schematic of a parabolic trough collector [2]

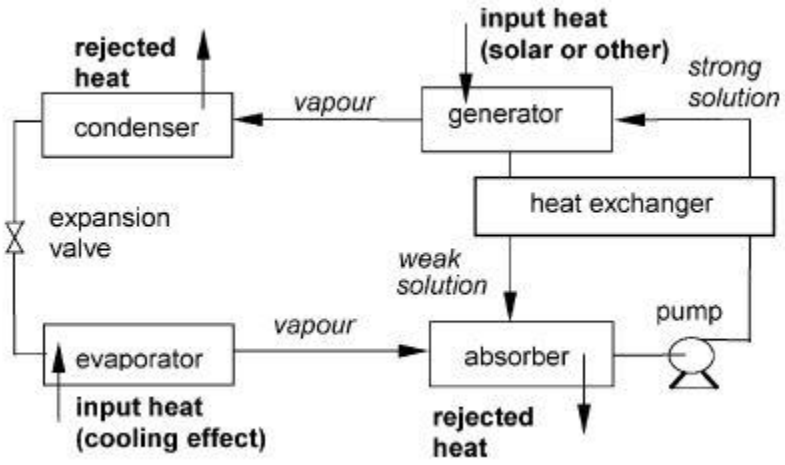

Fig. 4. Basic principle of solar refrigeration system [2]

However, solar energy is not available 24 hours. One good option in the application of solar energy is to make the solar energy collection system work as a supplementary source of heat for electricity generation. This helps the implementation bottom line by taking advantage of the "economy of installation". A heat recovery steam generation system, a device used to recover heat

from a hot flow source, is a good option for integrating intermittent solar energy with an actual thermal cycle. For example, integration of solar energy with a Combined Cycle (CC) power plant would help achieve a higher overall plant efficiency [11]. The coupling of Heat Recovery Steam Generator (HRSG) and the concentrating solar power (CSP) can effectively improve unit availability and dispatchability of solar energy and improve the operational flexibility of CC power plants [12, 13].

The Integration of CEWA Technologies' concentrating solar thermal technology with a diesel-fired power plant with a recuperator and a steam turbine, owned by the Mexican Federal Commission of Electricity (CFE in Spanish) was studied in this paper. The plant is located in Baja California, Mexico, which is a place with a high value of annual solar radiation. Direct Normal Irradiation (DNI) is a concept that represents the solar radiation strength and the amount of solar radiation received per unit area by a surface which is always perpendicular to the solar rays which come in a straight line from the direction of the sun. The DNI data for Hermosillo are shown in Figures. 5-6 and Table 1. A DNI of 887 W_{th}/m^2 was chosen as the standard peak solar radiation for Baja California, which is the average peak solar radiations in four quarters. The solar data shown above indicate that there are approximately 8.5 peak sun hours per day in Baja California

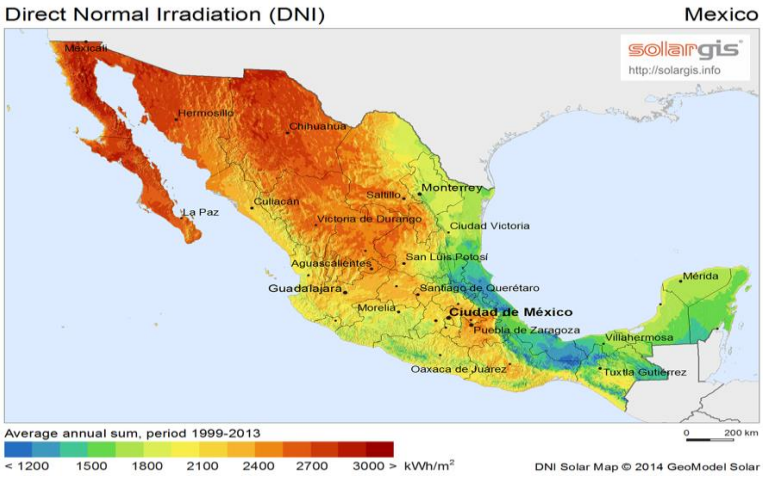

Fig. 5. Average annual direct normal irradiation in Mexico

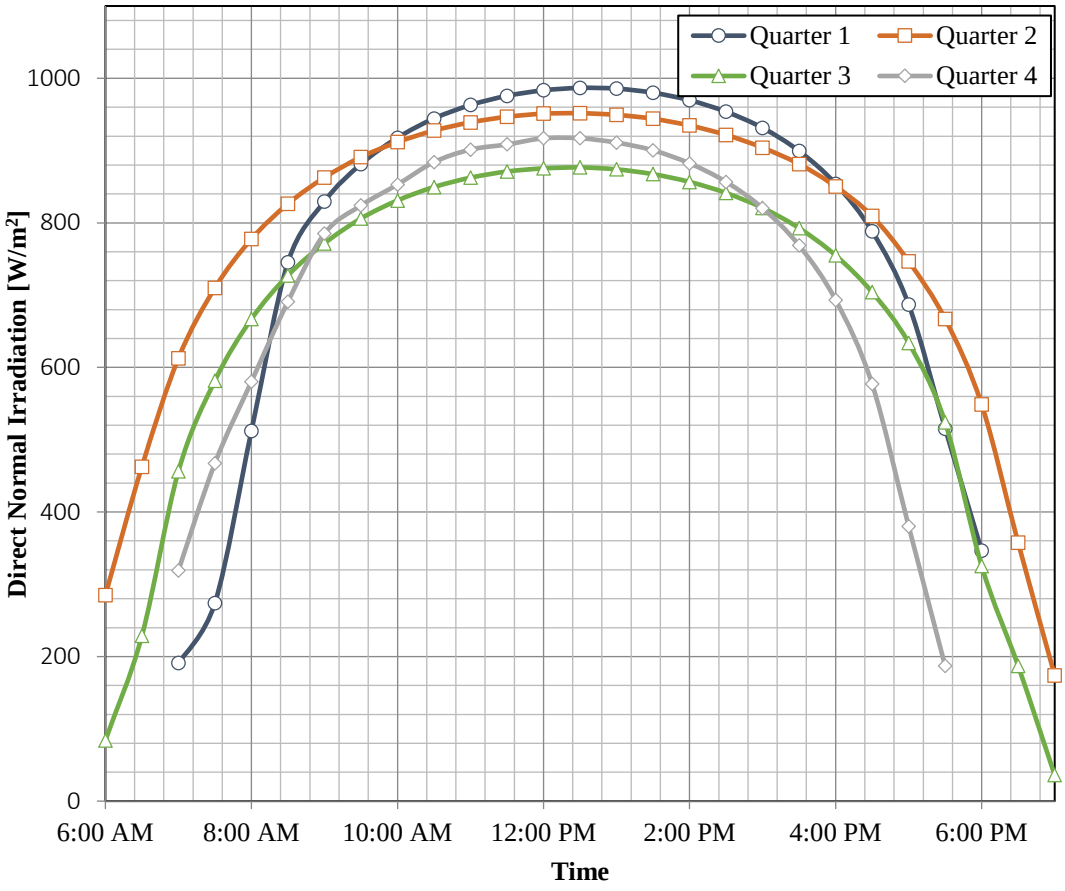

Fig. 6. Direct normal irradiation by hour during four quarters of a typical year in Baja California, Mexico

Table 1. Total DNI and Daily Peak Sun Hours from 2009 to 2012 in Hermosillo

Year	Year Total DNI [kWh/m^2]	Daily Peak Sun Hours [hrs./day]
2009	2,667.00	8.24
2010	2,814.87	8.70
2011	2,933.94	9.07
2012	2,752.77	8.49

area. Based on a standard DIN of 887 W_{th}/m^2 and 8.5 peak sun hours per day, the average annual solar irradiation is approximately 2752 kWh/ m^2.

This thesis presents a study on the integration of a CC power plant's HRSG with solar thermal energy. Simulation of different methods of integrating the solar thermal energy into the thermal plant was done by modeling with ASPEN Plus, maximizing solar conversion rates. Design data of the plant served as a reference for calculating net power output increase of the thermal plant after solar energy was integrated. Simulations were conducted under specific constraints on temperature of the feed water leaving a solar heat exchanger and the extraction ratio for extracting the feed water into the solar collection system. A comparison of solar conversion rates of different coupling approaches with different levels of solar thermal energy, under different flow rates of the feed water are showed. Optimal integration, which generate the largest solar conversion rate, is produced.

CHAPTER 2: Literature Review

Many investigations have been done on the integration of solar thermal energy with thermal plants, which are also called integrated solar combined cycle systems (ISCC). The first ISCC plant consisted of two 380 MW_e combined cycle power plants and a 5 MW_e parabolic trough solar field, with molten salts as the heat transfer fluid [14]. Currently, a number of ISCC plants have been built around the world, including the 75 MW_e Martin Next Generation Solar Energy Center in Indiantown Florida, the 20 MW_e ISCC Hassi R'me in Algeria and the 20 MW_e ISCC Kuraymat in Egypt [15-17]. Solar concentrating technologies currently applied at pilot and commercial plants are schematically showed in Figure. 7. Previous studies conduct discussion on different solar thermal technologies and setups for optimized operation. Peterseim et al. [15] performed an

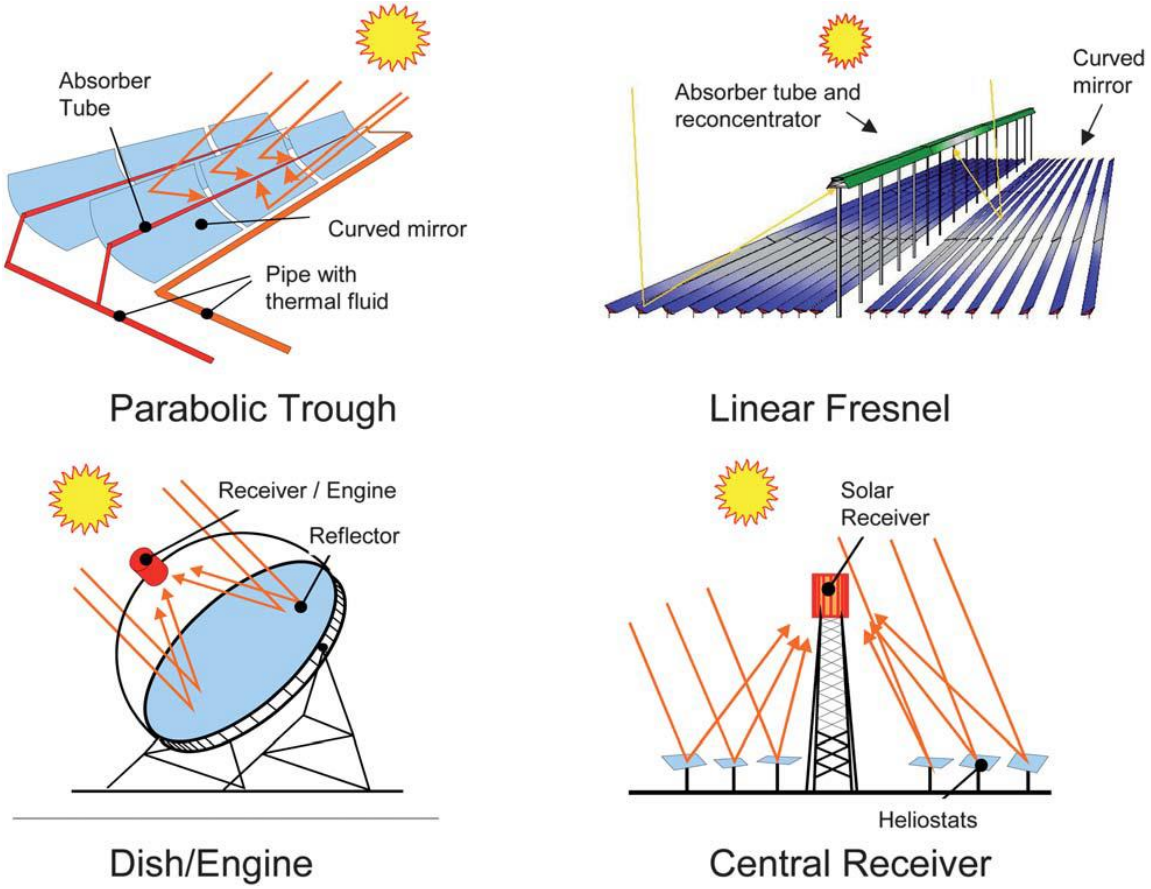

Fig. 7. Four solar concentrating technologies in use on CC plants [18]

assessment to identify the most suitable CSP technologies to hybridize with Rankine cycle power plants, using an Analytical Hierarchy Process (AHP). This study concluded that: (a) Fresnel systems should be used for feed water preheating, cold reheat steam production and <450 °C steam boost applications, (b) it is better to use solar towers rather than large dish technology when steam temperature are above 450 °C, (c) large dish technology is the only option to directly generate high pressure steam, above 580 °C. Kelly et al. [19] studied integration of plant designs, consisting of a General Electric Frame gas turbine and a three-pressure heat recovery steam generator. This study concluded that: (a) producing high pressure saturated steam and add it to a heat recovery steam generator is the most efficient way to use solar thermal energy, (b) there is a limitation on the quantity of high pressure steam transferred from the heat recovery steam generator to the solar steam generator, (c) higher cycle efficiency can be achieved through solar-fusion integration than by a solar-only parabolic trough plant. Rovira et al. [20] compared Heat Transfer Fluid (HTF) and Direct Steam Generation (DSG) under four different layouts and found that the configuration of only-evaporative DSG is the best choice due to its low irreversibility at the HRSG and high thermal efficiency in the solar field. Configurations of HTF and DSG are shown in Figure. 8. Nezammahalleh et al. [12] reported a techno-econo assessment of an ISCC system with DSG technology, compared with two conventional cases, and demonstrated that the ISCC system with DSG technology has the lower levelized energy cost (LEC) than the solar electric generating system and the ISCC system with HTF technology. Li et al. [13] analyzed a novel ISCC system with a two-stage solar input, as shown in Figure. 9. This study showed that the net solar-to-electricity efficiency could reach up to 30% in the novel two-stage ISCC system, which is higher than that of the one-stage ISCC power plant. Mokheimer et al. [21] provided a detailed investigation on the feasibility of integrating gas turbines of different generating capacities and

parabolic trough collectors of different areas, by using the PEACE simulation software. This research concluded that the integration of solar energy and gas turbines with capacities of less than 90 MW_e has a negligible increase in the overall levelized cost of electricity (LCOE). Furthermore,

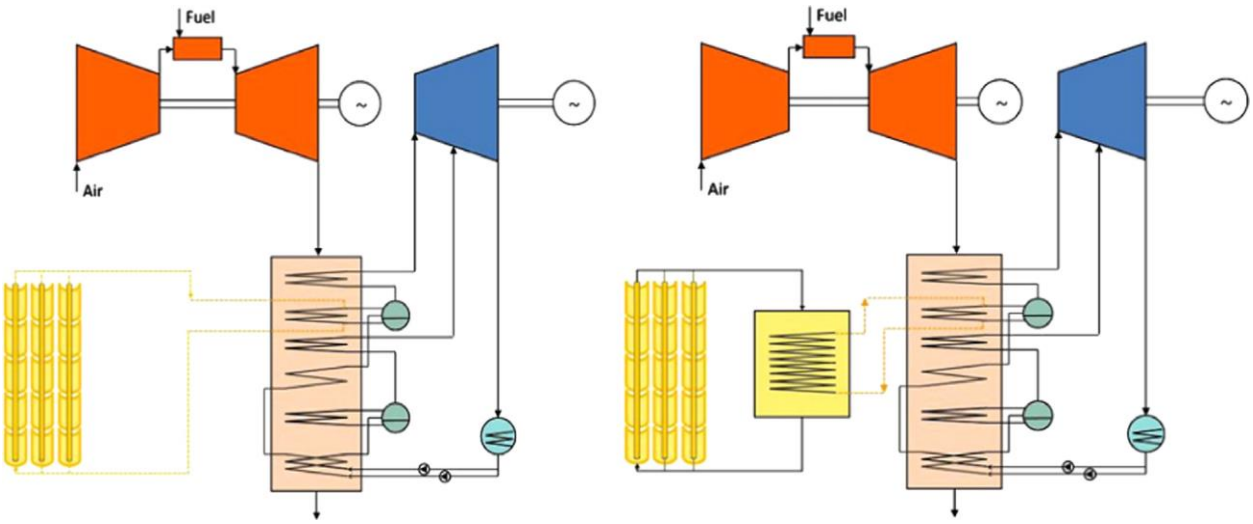

Fig. 8. Configurations of DSG (left) and HTF (right) [20]

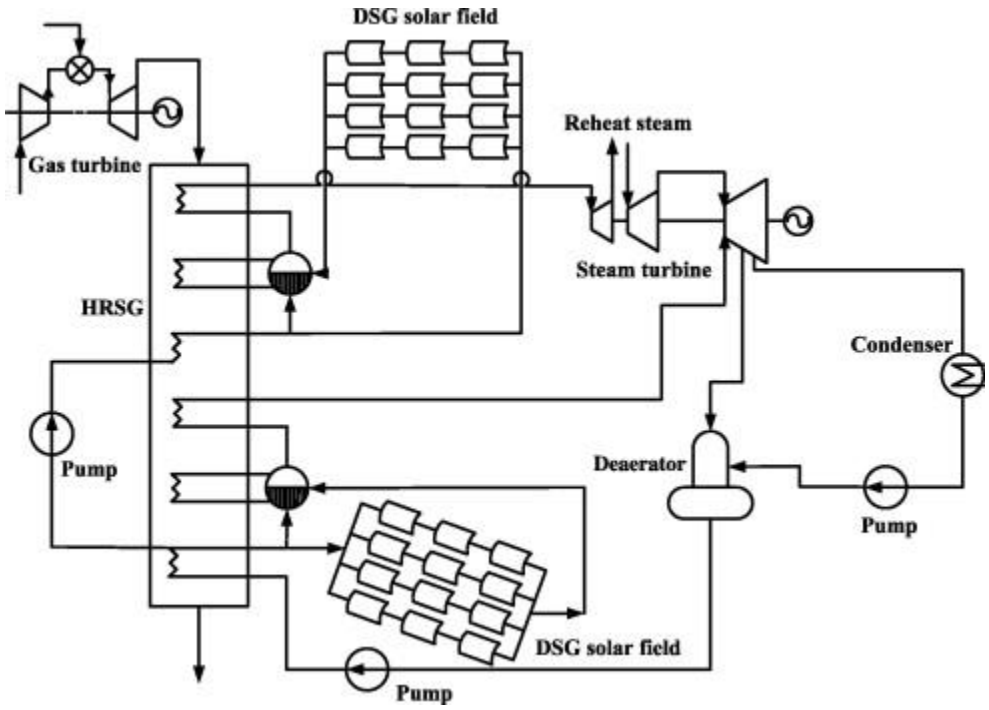

Fig. 9. Schematic diagram of ISCC power plant with two-stage solar input [13]

Montes et al. [22] analyzed a particular ISCC power plant which consists of a DSG parabolic trough field coupled to the bottom steam cycle of a CC power plant in two relevant examples: Almeria, with a Mediterranean climate, and Las Vegas, with hot and dry climate. The study showed that solar hybridization is better coupled with CC power plant in Las Vegas because of its frequent days with good solar radiation and higher ambient temperature. Jürgen et al. [23] analyzed four potential ISCC power plant projects in India, Egypt, Morocco and Mexico to identify the benefits of an ISCC power plant over an independent solar electric generation power plant and found optimized integration of the solar field and the power cycle. This study concluded that ISCC power plants can have less CO_2 emissions than independent solar electric generation, if the operation time is 24 hours per day. Mabrouk et al. [24] made an assessment of the solar thermal-to-electrical and radiation-to-electrical efficiencies and found the optimal setup of heat exchanger networks by using a general layout of an ISCC power plant. This investigation showed that: (a) the optimization algorithm produced a preference for higher temperature heat exchange over low temperature heat exchanger, (b) the thermal-to-electrical efficiency is reduced when the integrated solar heat rate increases, (c) increasing the mass flow rate of the solar source can increase the thermal-to-electrical efficiency. Philip et al. [25] constructed a computationally efficient ISCC model which includes detailed modeling of the heat recovery steam generator, by taking a wide variety of practical system constraints into consideration. This research concluded that there is an increase of the ISCC power plant's operating flexibility when the temperature of the heat transfer fluid coming out of the solar collection system is allowed to vary over operational time.

Additionally, research has been performed on the economic and environmental effects of ISCC power plants. Baghernejad et al. [26] carried out optimization of the investment cost of equipment and cost of exergy destruction through exergoeconomic principles and genetic

algorithms. This study concluded that the total amount of equipment investment cost and cost of exergy destruction could reduce by about 11% under optimum operation. Moore et al. [27] constructed a thermodynamic model to perform an engineering-economic analysis of an ISCC generator based on hourly solar resource data and hourly electricity prices, demonstrating that strong solar resources in the Southwest part of USA can make the LCOE of an ISCC power plants lower than that of stand-alone solar power plants. Bander et al. [28] estimated the LCOE and cost of carbon abatement for five locations in the USA which have different ambient temperature and solar resources by simulating hourly operations, and they concluded that the LCOE of ISCC can be reduced by 35%-40% relative to a stand-alone CSP plant. Mechthild et al. [29] studied an integrated solar combined cycle system in Egypt under the assumption of a CC power plant with identical total annual electricity production, with a parabolic trough collector field and a volumetric air receiver tower taken into consideration. Schematic diagrams of the ISCC power plant with trough solar field and an air tower are depicted in Figure. 10. The study found that the incremental cost and LEC of both technologies are similar. Hosseini et al. [30] identified the most

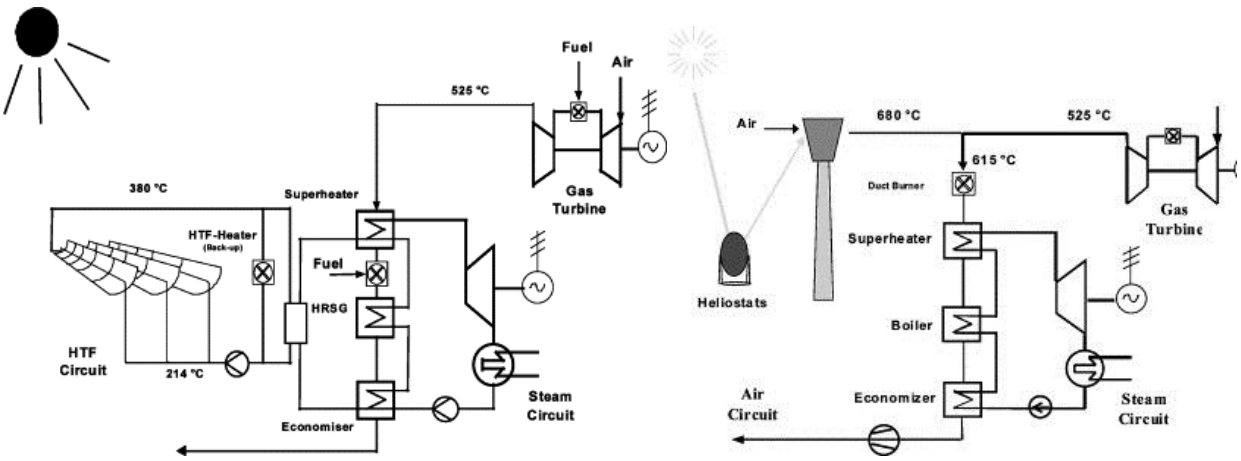

Fig. 10. ISCC with trough solar field (left) and ISCC with air tower (right) [29]

Suitable approach to build an ISCC power plant for the first solar power plant in Iran, based on an assessment of important parameters, including capacity factor, CO_2 emissions, investment level, operation and maintenance costs, price of fuel and thermal efficiency. The research reported that the ISCC system, with a 67 MW_e solar field, is the most suitable option, which can save 59 million in fuel consumption and make the LEC 33% lower than the comparable LEC of a gas turbine. Cavalcanti et al. [31] conducted an exergoeconomic and exergoenvironmental analysis of a cogenerative system which consists of a CC and a solar field through investigating the effect of the solar field on the performance of each component. The research concluded that the net produced electricity increases by 4.2% under the effects of a solar field, and the average cost rate per exergy unit of electricity gets 2.6% higher at the same time. Sairam et al. [32] performed economic, energy and exergy analyses on a conceptual ISCC power plant whose feed water leaving the high pressure economizer goes to the solar collection system for preheating and evaporation, and then be sent back to mix with the saturated steam leaving the high-pressure drum. This study showed that the solar collection system increases the power output of the plant by 7.84% and makes the LCOE 0.8 cents/kWh lower than that without solar field operation. Esmail et al. [33] conducted a thermo-economic comparative analysis of the integration of different CC power plants with three different CSP technologies, which include solar tower system, parabolic trough collector system and a linear fresnel reflector system, using PEACE simulation software. This investigation found that the integration of a gas turbine cogeneration plant of 50 MW_e with linear fresnel reflector system is the optimal configuration which provides a LEC of 0.051 cents/kWh while at the same time giving an annual 119 thousand tons reduction of CO_2.

CHAPTER 3: Integrated Solar Heat Recovery Steam Generator Cycle Model

The commercial software, ASPEN Plus, was used in this study to build computer models of the Rankine cycle side of a diesel engine-steam turbine CC. The Rankine cycle was integrated with CEWA's concentrating solar thermal energy technology. ASPEN Plus, as a process model, was able to incorporate mass and energy balances, and thermodynamic properties for predicting the thermal performance of the system [34].

3.1 Plant Description

The power plant of this study consists of a diesel engine and a HRSG system. Steam is generated in the HRSG system by recovering waste heat from the flue gas coming out of the diesel engine. Table 2 and Figure. 11 present design data of the combined cycle power plant located at Baja California, Mexico. Feed water comes into and out of the HRSG at a temperature of 95 °C and 276 °C, respectively. Water pressure increases from 0.165 bar to 8.88 bar before coming into HRSG. The temperature of the flue gas drops from 310 to 200 °C after heat exchange with the steam side of the HRSG. The feed water pressure drops from 8.88 bar to 0.165 bar after expanding in the steam turbine. As far as water properties is concerned, the feed water entering the HRSG is subcooled water while the feed water coming out of the HRSG becomes superheated water.

Table 2. Combined Cycle power plant design data

Parameters	Units	Values
Turbine Mechanical Efficiency	%	90
Turbine Isentropic Efficiency	%	85
Pump Isentropic Efficiency	%	75
Composition of Flue Gas entering HRSG under diesel engine full load		
O_2	%	10
CO_2	%	10
N_2	%	75
H_{2O}	%	5

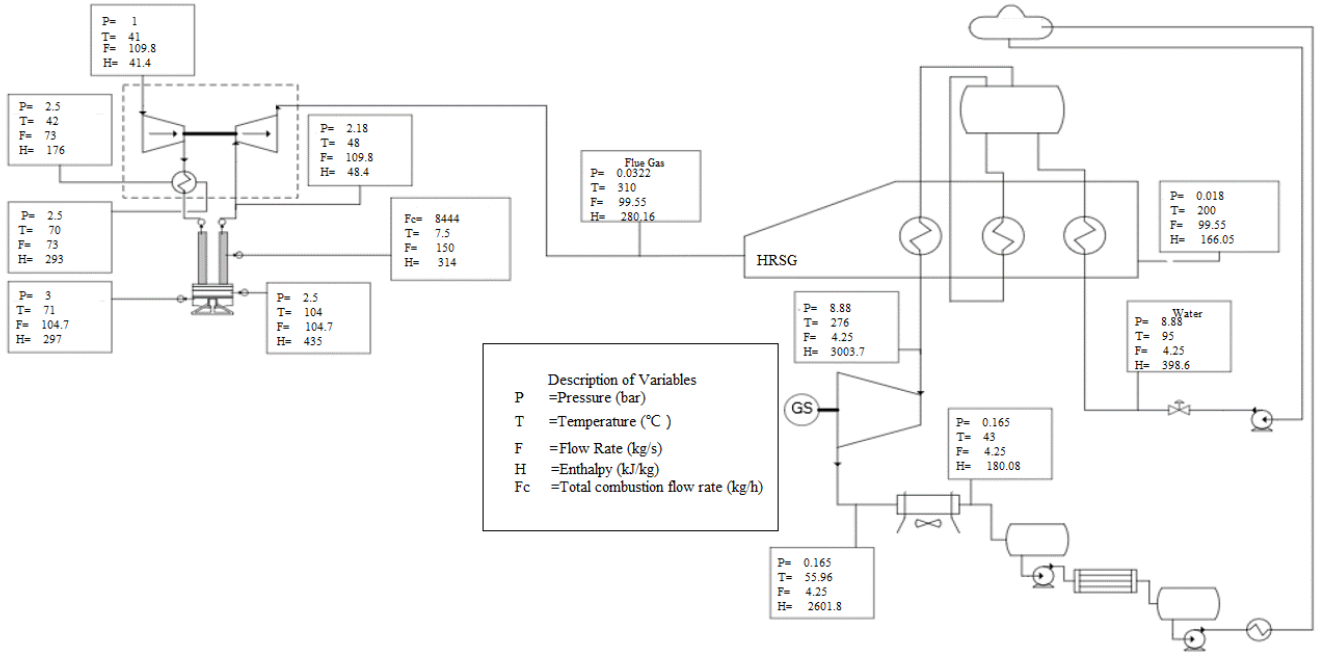

Fig. 11. Combined Cycle power plant design data

3.2 Solar Technology Description

The concentrating dish solar collector used in this study is manufactured by CEWA Technologies (see Figure. 12). In this design, the solar radiation is reflected by the solar dish onto a 2.5m diameter focal point at the receiver, and a HTF flowing through a heat exchanger in the receiver unit removes the captured heat from the solar collector. The required attributes of a HTF are non-or low toxicity, high specific heat, high thermal conductivity, high flash point and low viscosity at low temperature, environmentally friendly and economical. The following are some of the most commonly used HTF fluids and their properties [35]:

(1) Air

Air will not freeze or boil, and is non-corrosive. But its heat capacity is low, and is likely to leak out of collectors, ducts, and dampers.

(2) Water

Water is nontoxic and inexpensive. Its high specific heat and low viscosity makes it easy to be pumped. However, the boiling point of water is relatively low and the freezing point of water is relatively high. Additionally, water can be corrosive if the pH is not kept at a neutral level. Water with high mineral content can cause mineral deposits to form in the solar collector's tubing and plumbing system.

(3) Glycol/water mixtures

Glycol/water mixtures are typically made of 50/50 or 60/40 glycol-to-water ratios. Ethylene and propylene glycol are "antifreezes". These mixtures provide effective freeze protection as long as the proper antifreeze concentrations is maintained. Antifreeze fluids degrade over time and normally should be changed every 3-5 years. These types of systems are pressurized, and should

only be serviced by a qualified solar heating professional. Besides, these mixtures can be heated up to 230 ℃.

(4) Hydrocarbon oils

Hydrocarbon oils have a higher viscosity and lower specific heat than water. The basic categories of hydrocarbon oils are synthetic hydrocarbons, paraffin hydrocarbons, and aromatic refined mineral oils. Synthetic hydrocarbons are relatively nontoxic and require little maintenance. These types of HTFs have the highest working temperature which can be up to 350 ℃.

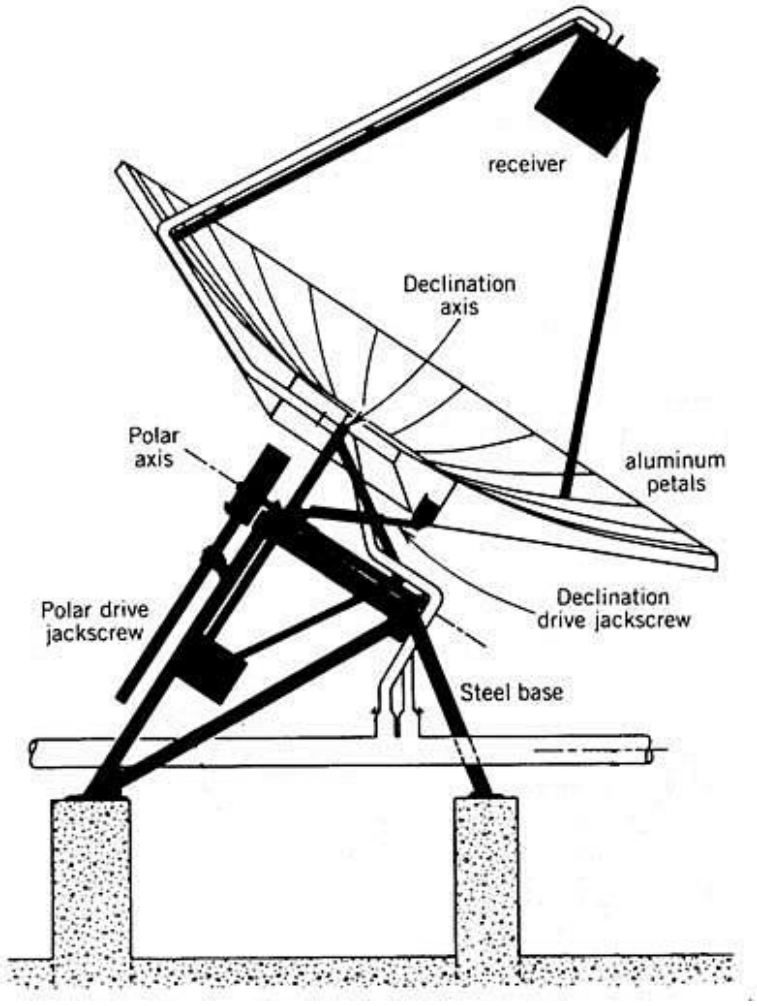

Fig. 12. Sketch of CEWA technologies' concentrating solar collector

Based on the design data of the original CC power plant of this study, the temperature range of the feed water is from 95 ℃ to 276 ℃. The working temperature of HTF for this application should be close to and higher than 276 ℃. So a Dynalene SF, a hydrocarbon oil produced by Dynalene, Inc, was chosen as the HTF here for the reason that it is thermally stable at working temperatures up to 315 ℃ while at the same time ready and cost-effective through North America. Properties of Dynalene SF are listed in Table 3. Table 4 summarizes technical data for the solar collection system. With a peak DNI value of 887 W_{th}/m^2 of incident radiation, a parabolic collector surface area of 43 m^2 and the thermal output during peak sun hours of 30 $kW_{th,}$ an estimated solar-heat efficiency η can be calculated for this collector as:

$$\eta = \frac{887\ \mathrm{Wth/m^2} \times 43\ \mathrm{m^2}}{30\ \mathrm{kWth}} = 78.7\%$$

Table 3. Properties of Dynalene SF

Composition	Synthetic alkylated aromatics
Appearance	Clear, light down
Odor	Low odor
Pour Point	-60 ℃ (-76 ℉)
Boiling Point	>330 ℃ (>626 ℉)
Flash Point	180 ℃ (356 ℉)
Autoignition Temp	330 ℃ (626 ℉)
Max Film Temp	340 ℃ (644 ℉)
Max Fluid Outlet Temp	315 ℃ (600 ℉)
Min Pumpability Limit	-10 ℃ (14 ℉)
C_p (kJ/kg)	0.0037×T (℃)+1.8936

Table 4. Main technical data of solar collection system

Solar Dish Technical Data		
Parameter	Unit	Value
Solar Dish Geometry		
Total Clear Aperture	m^2	43
Concentration Ratio @ Focus Point	-	700
Focus Point	m	2.5
Dish Diameter	m	7.65
Heat Receiver Coil Pipe Size	-	3/8'' Schedule 40
Heat Receiver Coil Pipe Length	m	58
Solar Dish Thermodynamic Characteristic		
Maximum Temperature	℃	500
Peak Thermal Output @ 887W/ m^2 Irradiation	kW_{th}	30
Heat Transfer Fluid (HTF) Data		
HTF Brand	-	Dynalene SF
HTF Working Temperature Range (Closed System)	℃	0 - 315
Density @ 200℃	kg/m^3	756
Specific Heat @ 200℃	kJ/kg·K	2.625
Thermal Conductivity @ 200℃	W/m·K	0.1208
Viscosity @ 200℃	mPa·s	1.00
Expansion From 50℃ to 350℃	%	40
Solar Dish Installed Cost		
Installed Cost per Dish	$ (U.S.)	35,000

3.3 Model Description

One of the major assumption used in the model development is that the diesel engine always operates at full load; thus, diesel engine load cycling was not taken into consideration. Thus, the computer model of the original CC power plant simplified into a single pressure HRSG with a turbine was shown. Figure. 13 shows a detailed model process diagram for the steam cycle of the CC power plant (no solar thermal energy input). Pumps were also simplified into a single pump which increases the pressure of the feed water from 0.165 bar to 8.88 bar. The HRSG includes three counterflow heat exchangers. The process unit labeled "PREHEAT", "EVAPORA" and "SUPREHE" represents the preheater, evaporator and superheater of the HRSG respectively.

Based on the design data of the CC power plant, the "Design" option was chosen in the calculation mode for setup of the heat exchangers in the model, allowing that only inlet and outlet temperatures of the HRSG are known. The temperatures of the feed water entering the preheater and leaving the superheater is set to 95 °C and 276 °C, respectively. The temperature of the feed water leaving the evaporator is near the saturated temperature of water at the pressure of 8.88 bar, and the vapor fraction of steam leaving the evaporator was set to 1. So water just changes from saturated water to saturated steam without being superheated, which can make simulation easy to converge in the evaporator. The parameters selected in ASPEN Plus for this model of a CC power plant in the property database for water is STEAMNBS, and the property database for the flue gas is SR-POLAR. The true components is the simulation approach while the 3-no correction is chosen for water solubility method. Table 5 describes the technical data for all process units, derived from the simulation of the CC power plant in ASPEN Plus. UA is the value of the heat transfer coefficient multiplied by the heat transfer area, which decides properties of a heat exchanger. UA of a heat exchanger was calculated given the heat duty, H, maximum temperature difference, ΔT_{max}, and the minimum temperature difference ΔT_{min} of inlet and outlet temperature giving:

$$UA = \frac{H \times \ln \frac{\Delta T_{max}}{\Delta T_{min}}}{\Delta T_{max} - \Delta T_{min}}$$

The results shown in Figure. 13 are consistent with the design data within negligible error. The existing of other chemical components with just a small amount like alkanes in the original CC power plant leads to the difference of outlet temperature of the flue gas leaving HRSG.

Two different options for incorporating the solar energy into the CC power plant were investigated and modeled in this study. Option 1 corresponds to heating all feed water in the circulation loop (see Figures.14-17). Option 2 corresponds to heating a part of the feed water

extracted out of the circulation loop, and adding it back to the circulation system (see Figures. 18-23). “SOLAR” represents the solar heat exchanger, a countercurrent heat exchanger, where feed water gets heat by the HTF. “EXTRACT” represents the process unit to extract the feed water from the circulation and “MIXER” represents the process unit to mix the feed water in the circulation and water leaving the solar heat exchanger. Option 1 which offers options to heat the feed water at different locations and Option 2 which offers options to extract feed and return feed water at different locations were analyzed.

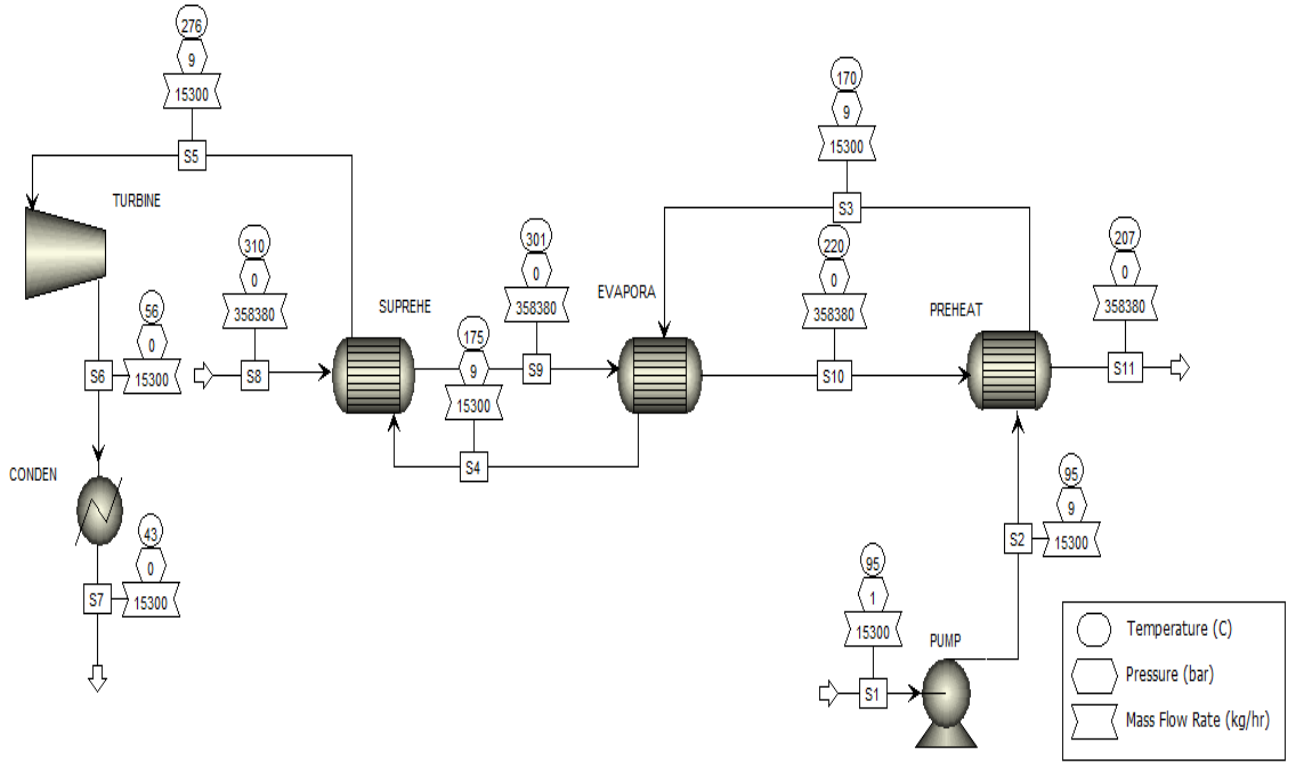

Fig. 13. Process diagram of the CC power plant based on design data

Table 5. Technical data of all process units in the CC power plant

Flow Rate (kg/s)	
Stream S1	4.8875
Stream S8	99.5500
UA in Each Heat Changer (J/s·K)	
Preheater	17796.8
Evaporator	106401.0
Superheater	13855.8
Net Power Work (MW)	
Pump	0.00435
Turbine	2.24870
Net power output	2.24400

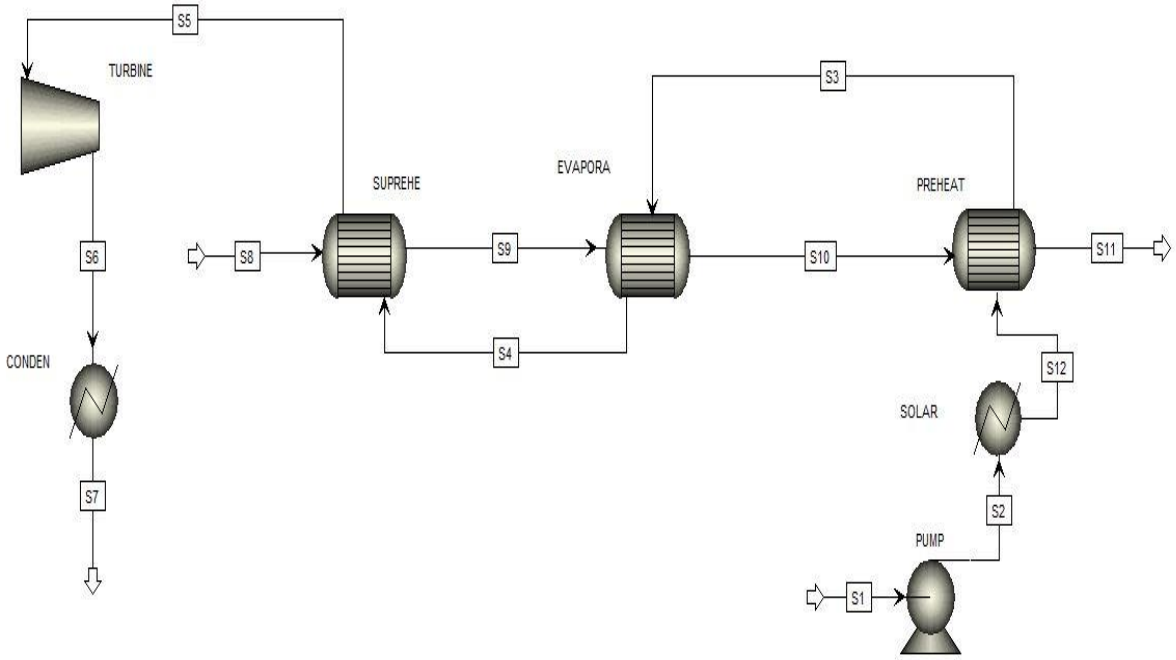

Fig. 14. Option 1, heating before the preheater

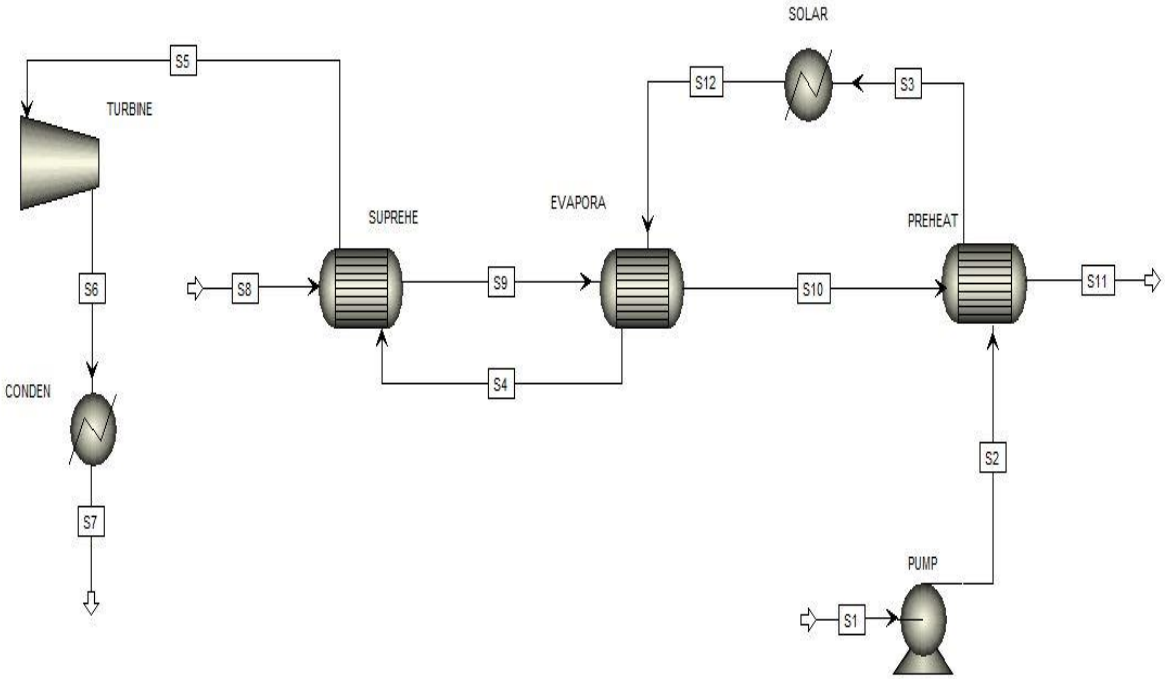

Fig. 15. Option 1, heating before the evaporator

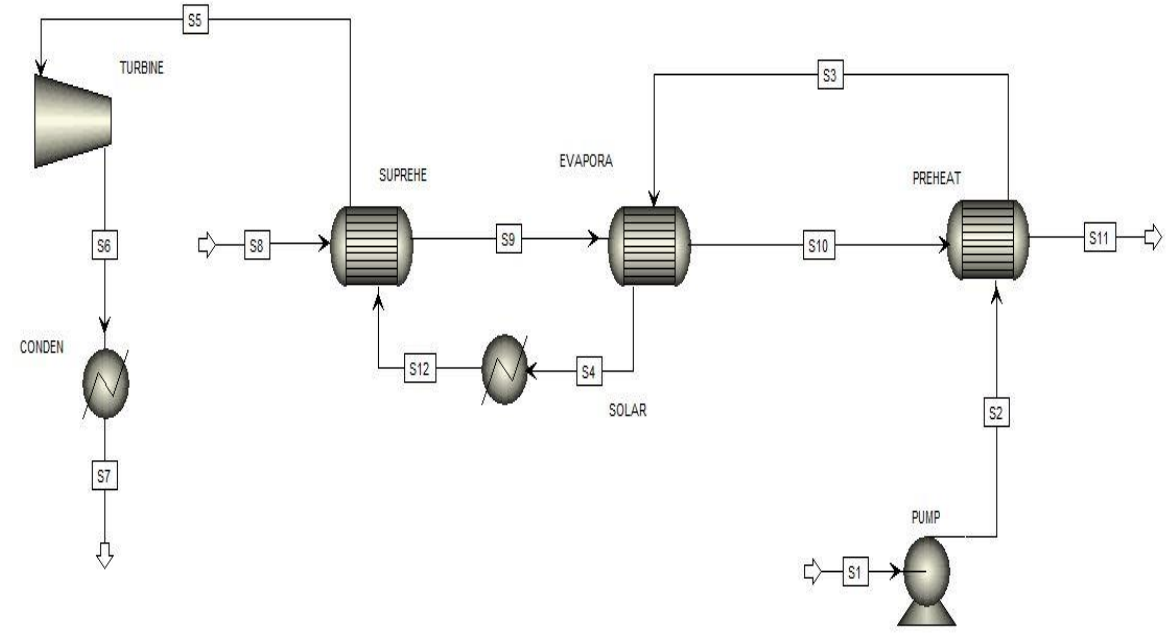

Fig. 16. Option 1, heating before the superheater

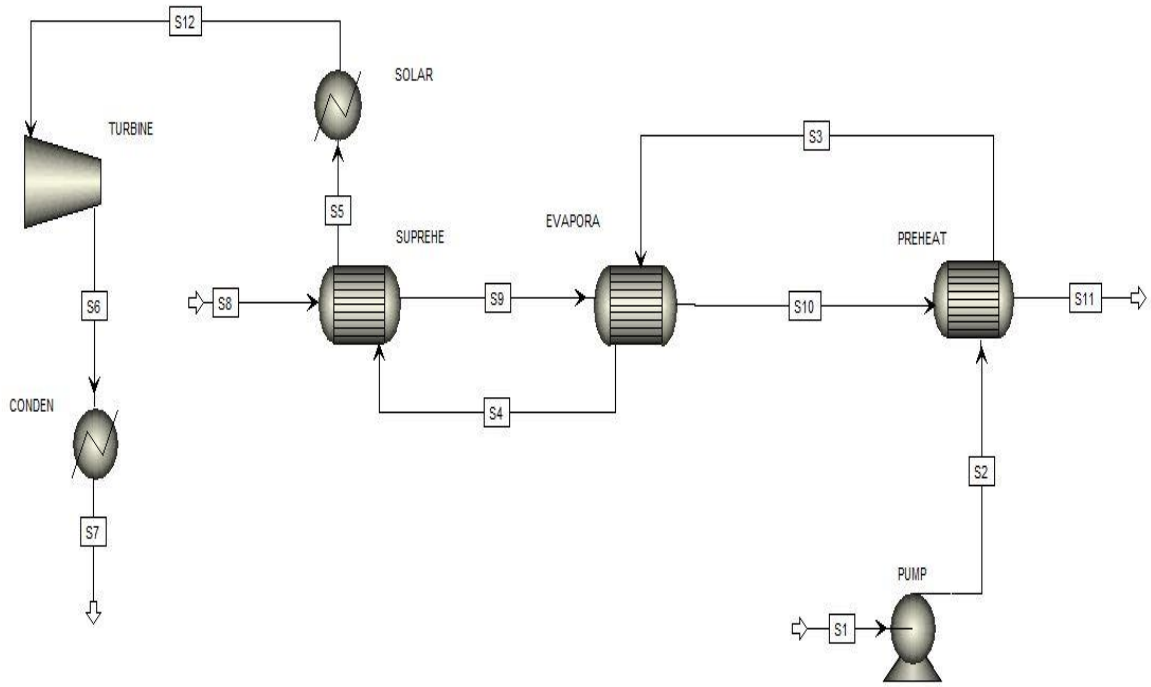

Fig. 17. Option 1, heating after the superheater

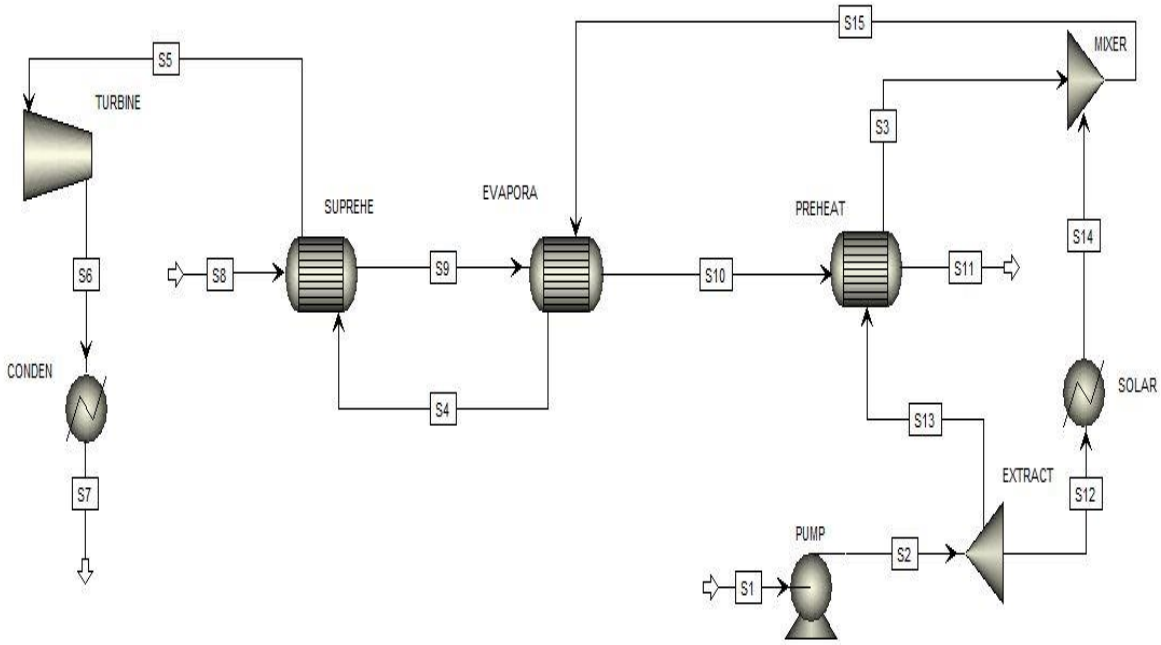

Fig. 18. Option 2, extraction from before the preheater to after the preheater

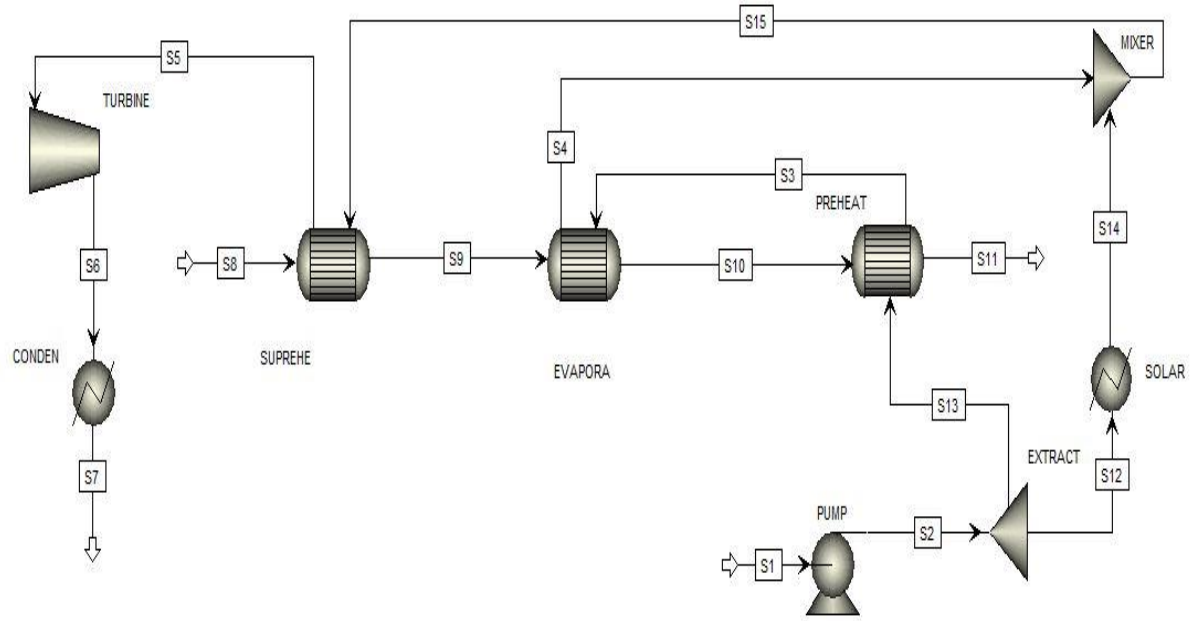

Fig. 19. Option 2, extraction from before the preheater to after the evaporator

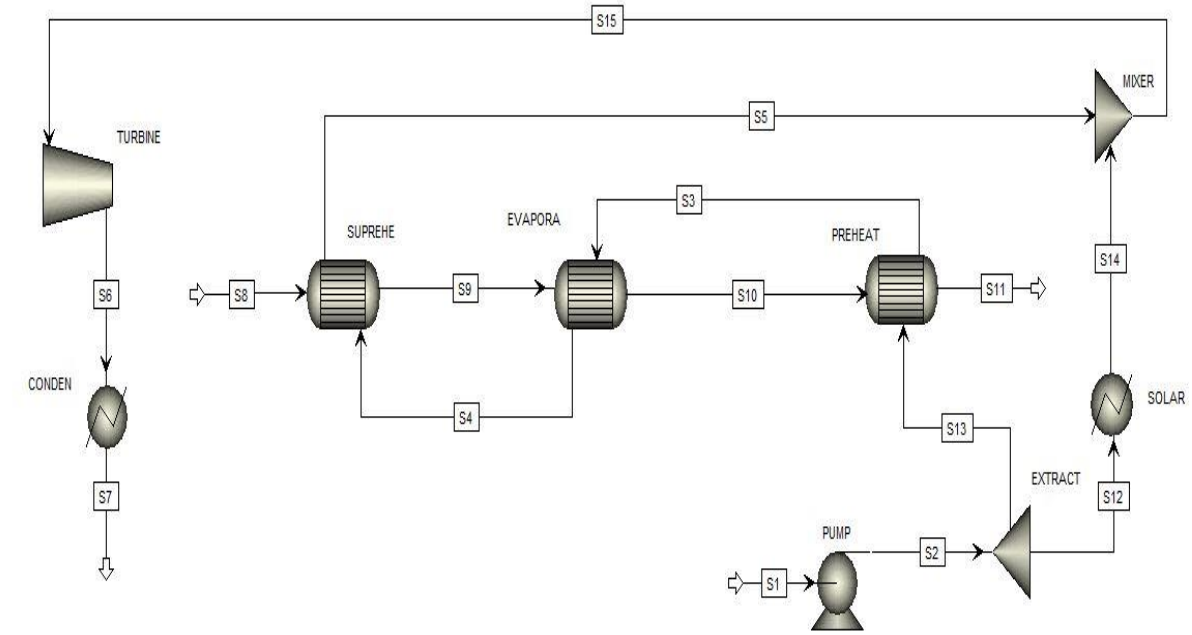

Fig. 20. Option 2, extraction from before the preheater to after the superheater

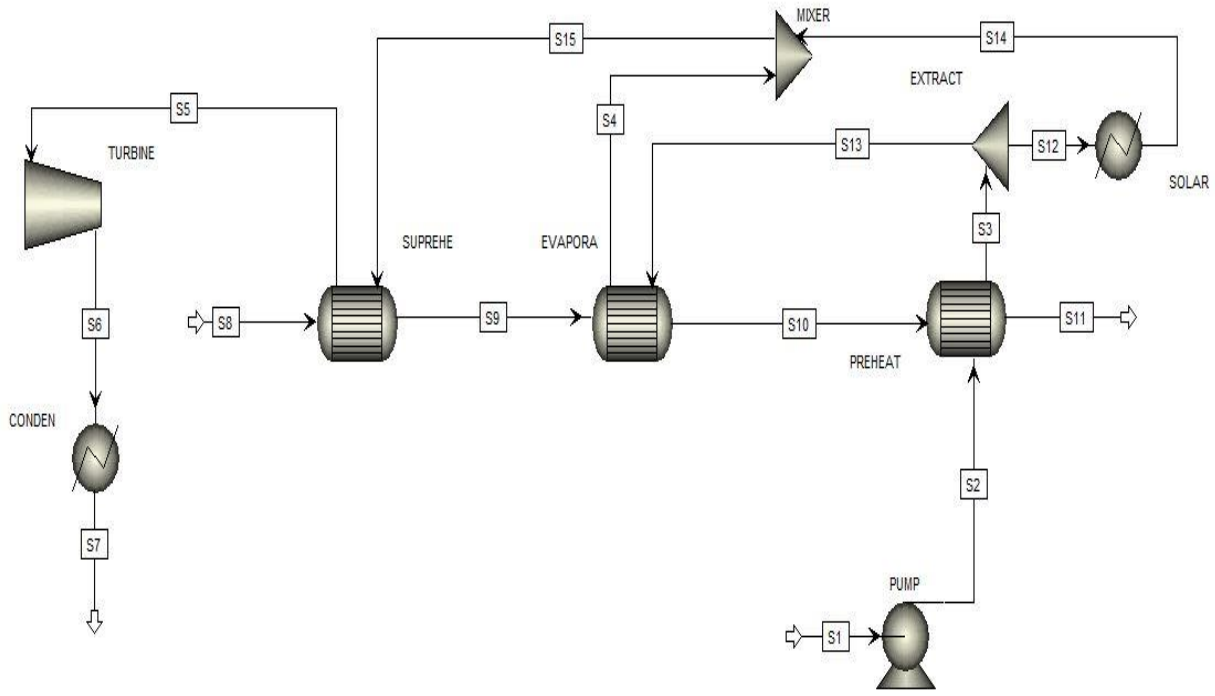

Fig. 21. Option 2, extraction from before the evaporator to after the evaporator

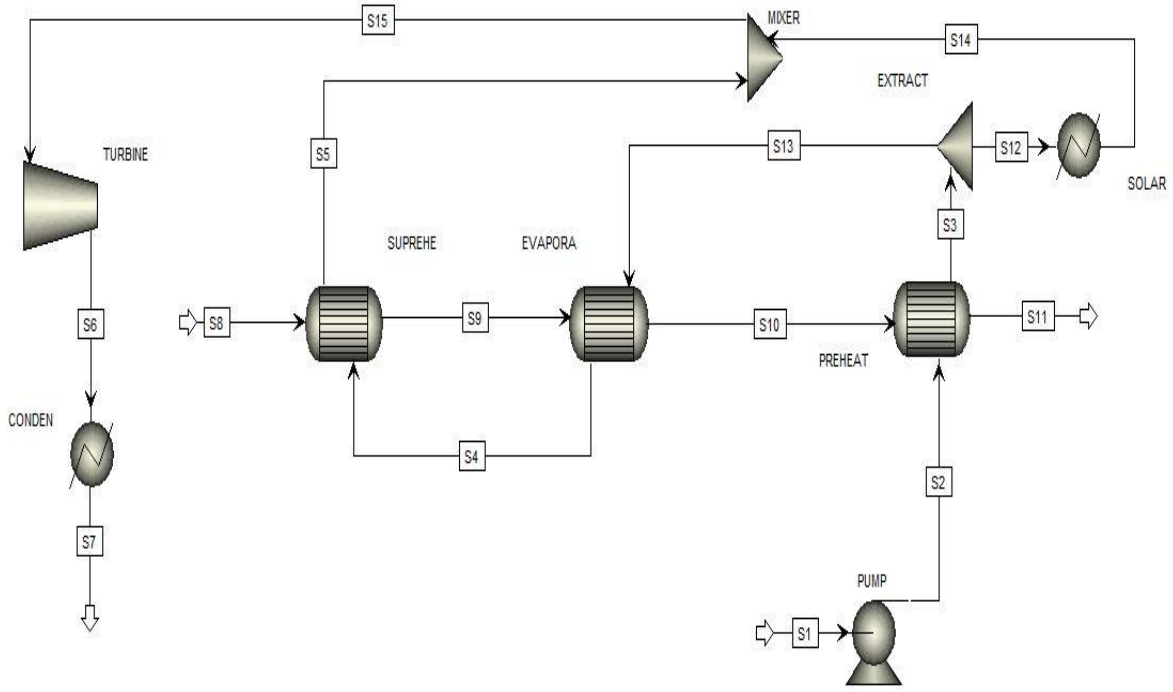

Fig. 22. Option 2, extraction from before the evaporator to after the superheater

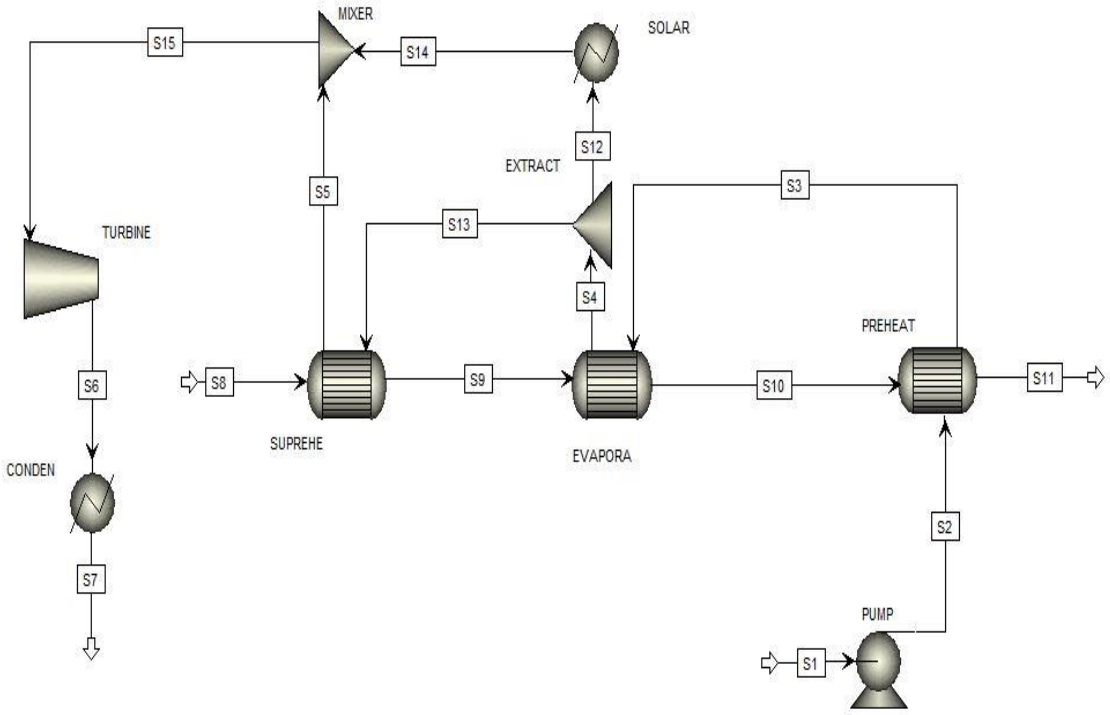

Fig. 23. Option 2, extraction from beforethe superheater to after the superheater

For the integrated solar-CC plant model built in ASPEN Plus, the following assumptions were made:

(a) Turbine mechanical efficiency, turbine isentropic efficiency, flue gas composition and UA of each heat exchanger were kept the same as the assumed values used in the baseline model of the CC power plant.

(b) The composition and temperature of the flue gas leaving the diesel engine change with the load of the diesel engine, which can affect heat duty in each of the heat exchanger and temperature distribution in the entire power plant cycle. In this study, it was only considered the situation when the diesel engine operates at full load. Thus, the properties of the flue gas were left constant and the Rankine cycle was the only portion taken into consideration.

(c) The UA of the heat exchangers can change with the flow rate of any side within the heat exchanger. Simulation were conducted at constant UA values. In this case, the extraction ratio of

the feed water in Option 2 cannot exceed 0.5, warranting a small change of flow rate within the heat exchangers. The extraction ratio of the feed water in Option 2 was set to be higher than 0.01 for the reason that extraction ratios of the feed water lower than 0.01 is hard to achieve in practice.

(d) According to the main technical data of the solar collection system, 315 ℃ is the highest temperature which the HTF can handle. Thus the temperature of the feed water leaving the solar heat exchanger was set to be lower than 295 ℃, to warrant enough temperature difference between the feed water and HTF for effective heat transfer in the counterflow heat exchanger.

(e) The parameters selected in ASPEN Plus for the models of the CC power plant integrated with solar thermal energy, the property method for water, property method for flue gas and true components, water solubility method were kept at the same parameters of the models of the CC power plant.

CHAPTER 4: Simulation Results and Discussion

A net power output increase parameter was defined which is the difference between net power output of the CC power plant and net power output of the CC power plant integrated with solar thermal energy. A solar conversion rate was introduced also, which is the ratio of the net power output increase over the value of solar thermal energy integrated. The results and comparison of solar conversion rates under different values of solar thermal energy for different coupling approaches of integrating solar thermal energy into the CC power plant were presented. The amount of solar energy analyzed in this study ranges from 480, 720, 960 to 1440 kW_{th}, which is 21, 31.5, 42 and 63% of the net power output of the original CC power plant. Additionally, solar conversion rates of the CC power plant integrated with solar thermal energy at conditions of increased flow rate of the feed water are also discussed in this chapter.

As discussed in Chapter 3, two different options of adding solar energy into the CC power plant were investigated. Option 1 includes different locations to heat the feed water, and Option 2 includes different locations to extract the feed water as well as different locations to return the feed water. For convenience, all the coupling approaches of integrating solar thermal energy into the CC power plant are numbered, indicated in Table 6. Option 1 includes Methods (1)-(4), and Option 2 includes Methods (5)-(10).

With Option 2, the feed water needs to be extracted from the circulation loop. In this case, different extraction ratios of the feed water to the solar heat exchanger which have an impact on the temperature of the feed water leaving the solar heat exchanger, leading to different solar conversion rates. The maximum solar conversion rate each method can attain needs to be found as well as the corresponding extraction ratio of the feed water to the solar heat exchanger which is regarded as the optimal extraction ratio. Additionally, the maximum solar conversion rate which

determines the performance of a method included in Option 2 is used for later comparison. A range of extraction ratio of the feed water to the solar heat exchanger was explored from 0.01 to 0.5, based on assumption (c). A sensitivity analysis using the Model Analysis Tools in Aspen Plus was

Table 6. List of all the methods of integrating solar thermal energy

Option 1	Heating point	
Method (1)	Before preheater	
Method (2)	Before evaporator	
Method (3)	Before superheater	
Method (4)	After superheater	
Option 2	**Extraction point**	**Returning point**
Method (5)	Before preheater	After preheater
Method (6)	Before preheater	After evaporator
Method (7)	Before preheater	After superheater
Method (8)	Before evaporator	After evaporator
Method (9)	Before evaporator	After superheater
Method (10)	Before superheater	After superheater

used to calculate net power output of the CC power plant integrated with solar energy at each step, for range of the extraction ratio of the feed water to the solar heat exchanger. Figure. 24 shows how net power output varies with extraction ratio for Methods (5)-(10) when the solar energy input is 480 kW_{th}.

For all the Methods (5)-(10), with solar energy at 480 kW_{th}, the net power output decreases when the extraction ratio is increased. The big step in Figure. 24 (a) is due to the feed water leaving MIXER, a mix of saturated water and steam. The temperature of this mixture is always 175 °C at a constant pressure of 8.88 bar. Thus the extraction ratio of the feed water to the solar heat exchanger affects the ratio of saturated steam leaving MIXER but has no impact on the temperature of the mixture, which is related to its exergy. Exergy is the energy that is available to be used. The almost constant exergy of the mix leads to a very small change in the net power output of the CC power plant integrated with solar thermal energy. Additionally, the solar conversion rate also

decreases with an increasing extraction ratio of the feed water to the solar heat exchanger when the net power output of the CC power plant integrated with the solar thermal energy decreases (with an increasing extraction ratio of feed water). There may be a point where there may not be enough water to cool down the flue gas if the extraction ratio of the feed water is too high, resulting in heat from the flue gas not completely recovered. This suggests that the extraction ratio should be as low as possible for a maximum solar conversion rate.

It was found that the temperature of the feed water leaving the solar heat exchanger increases when the extraction ratio of the feed water to the solar heat exchanger decreases. There is a limit for the outlet temperature of feed water which is 295 ℃ discussed in assumption (d) in Chapter 2. In this way, the extraction ratio of the feed water to the solar heat exchanger at a temperature of 295 ℃ should allow for the lowest extraction ratio that will lead to the maximum solar conversion rate. This extraction ratio would be the optimal extraction ratio. This situation also happens for Methods (5)-(10) when the solar input is 720, 960 and 1440 kW_{th}. The Design Specs of Flowsheeting Options in ASPEN Plus is a tool used to find the value of a certain parameter which can generate a desired optimal value of any other process parameter in the simulation. The optimal extraction ratio of Methods (5)-(10) included in Option 2 was found with solar energy input of 480 to 1440 kW_{th} by using Design Specs of Flowsheeting Options in ASPEN Plus. The solar conversion rate of Methods (5)-(10) refers to the maximum solar conversion rate each method can achieve.

The solar conversion rates of Methods (1)-(10) when the solar thermal energy is 480, 720, 960 and 1440 kW_{th} are shown in Figure. 25.

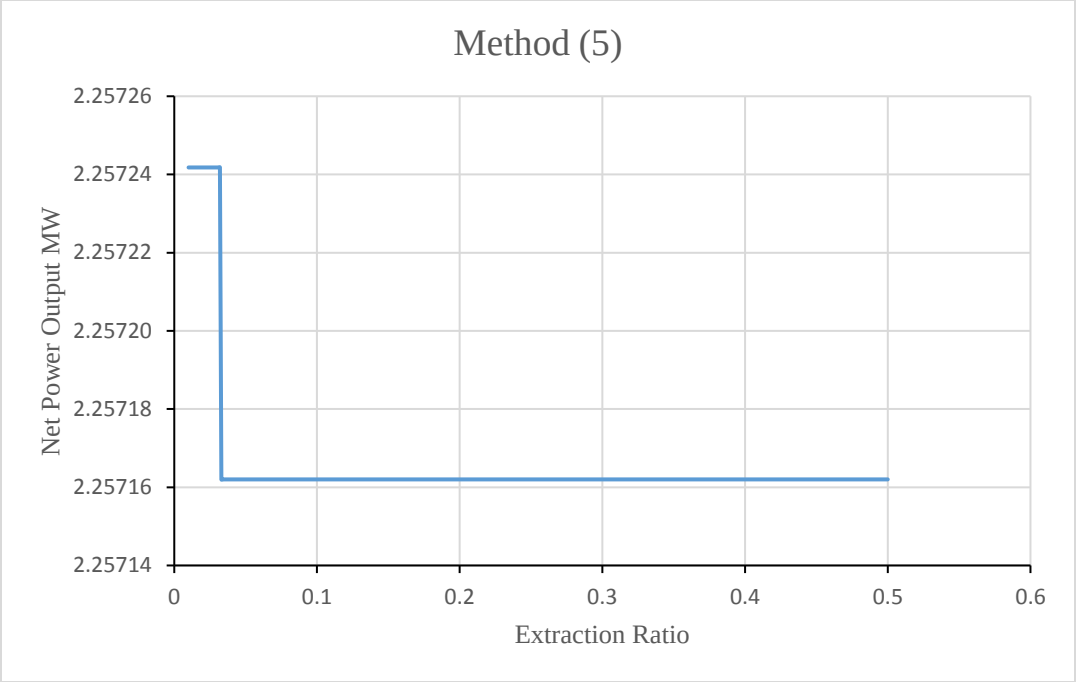

Fig. 24 (a)

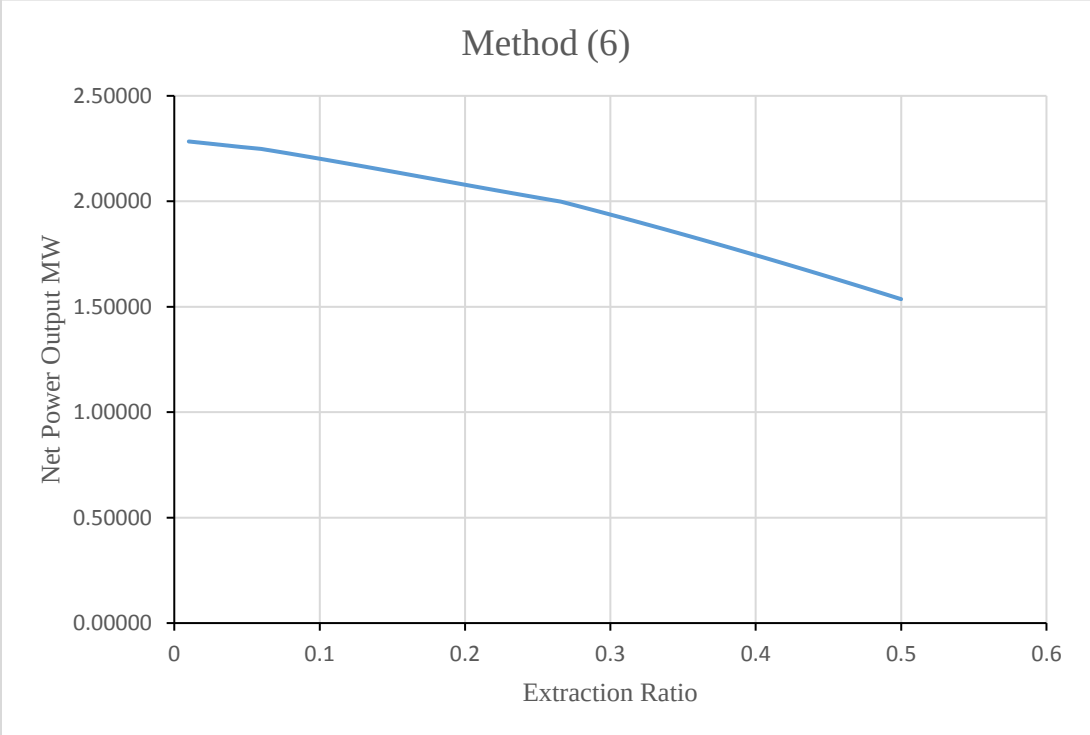

Fig. 24 (b)

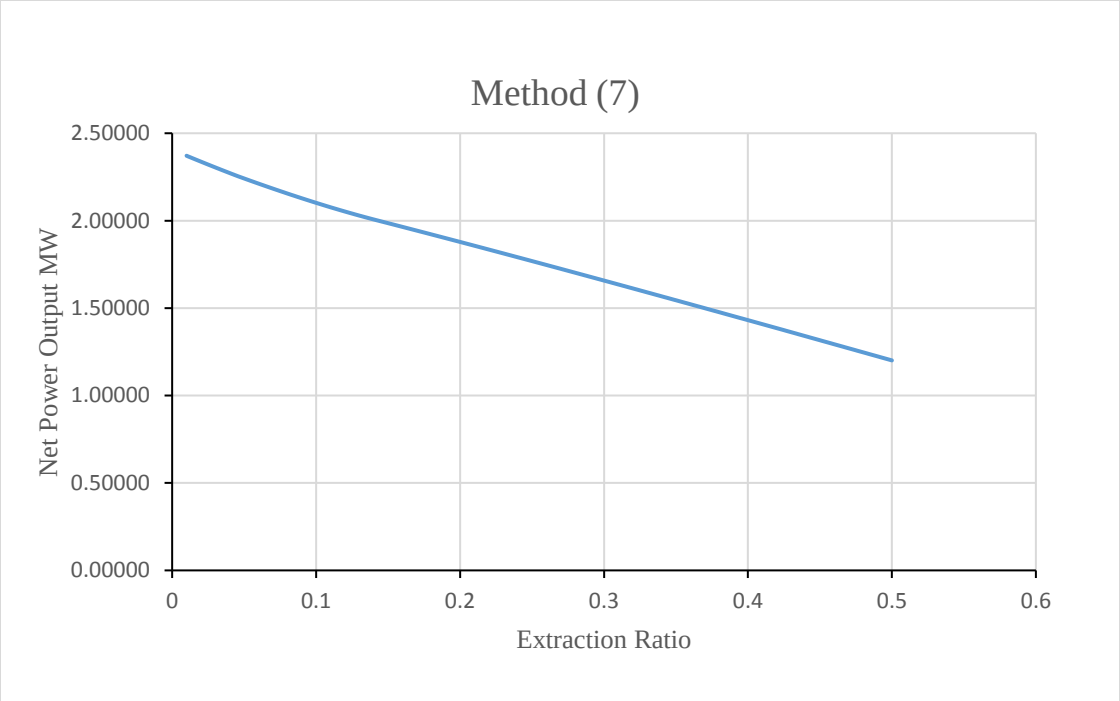

Fig. 24 (c)

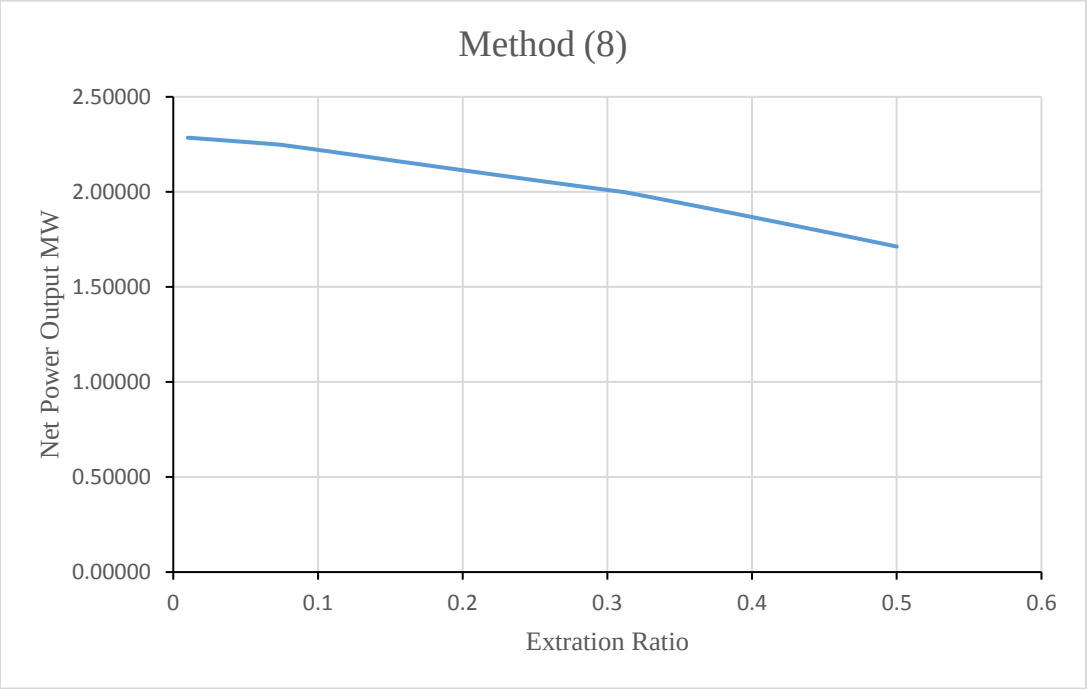

Fig. 24 (d)

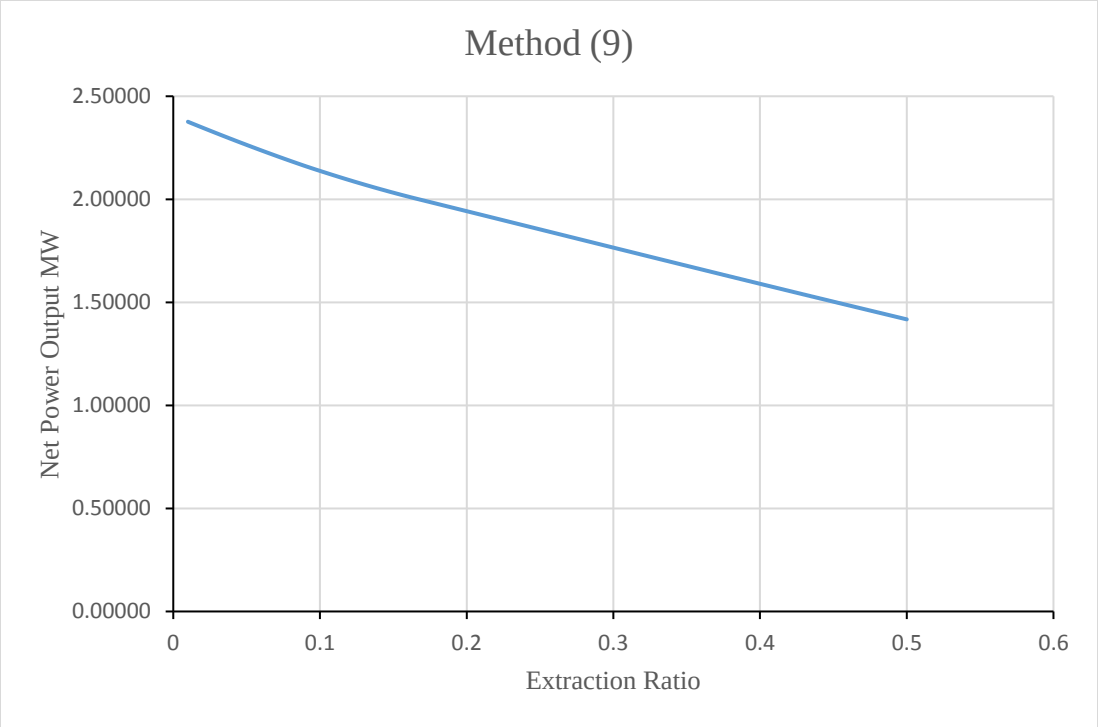

Fig. 24 (e)

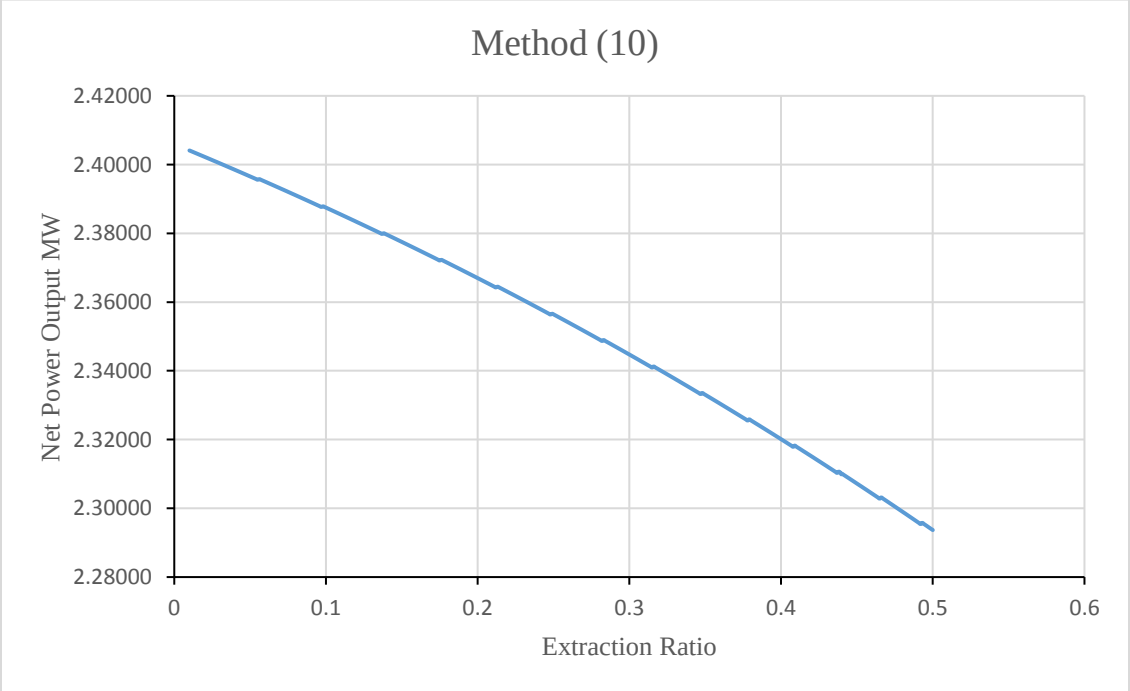

Fig. 24 (f)

Fig. 24. (a)-(f) Net power output under different extraction ratio with the solar energy of 480 kW

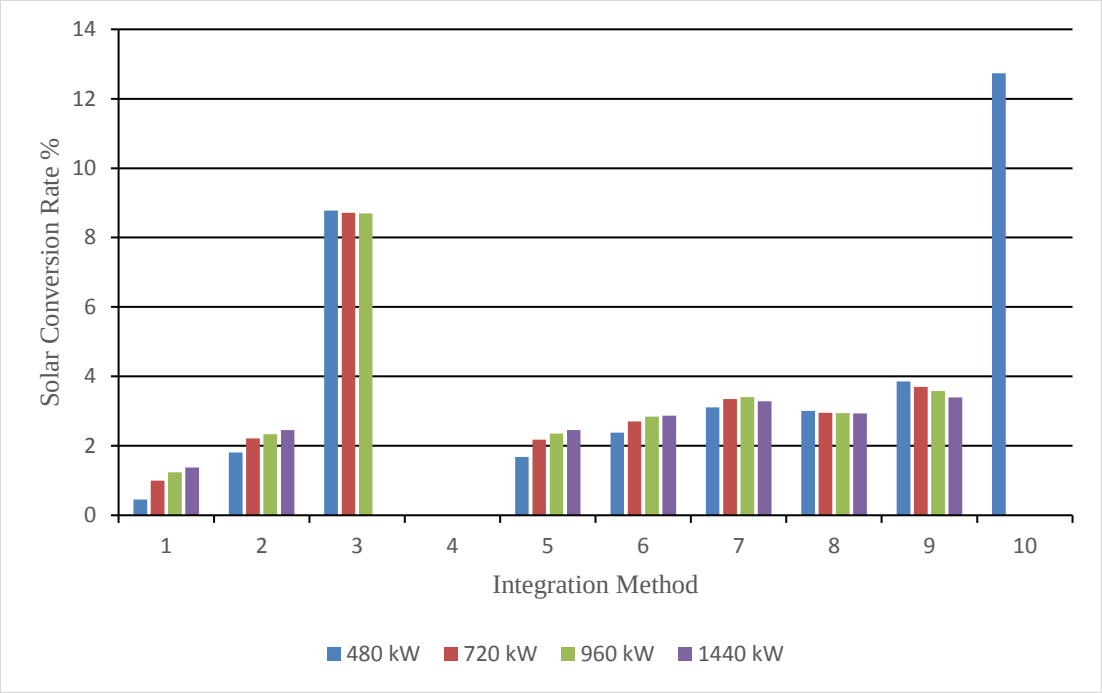

Fig. 25. Solar conversion rates of different methods, with different values of solar input

It can be observed that the solar conversion rate does not exist under certain options or input level of solar thermal energy. This implies that the solar integration, under these conditions, results in the extraction ratio of the feed water to the solar heat exchanger and the temperature of the water/steam leaving the solar heat exchange to exceed the limits discussed in assumption (d) in Chapter 2, or there is a decrease in the net power output of the CC power plant after solar thermal energy is integrated, due to impact on the performance. The integration is not practical under Method (4), for all values of solar input, due to the temperature of the feed water leaving the superheater being too high, making it easy for the temperature of the feed water leaving the solar heat exchanger to exceed the imposed limit of 295 °C. Additionally, the integration is not attractive under Method (3) with a solar energy input of 1440 kW_{th} because the amount of solar energy is large enough to heat the feed water leaving the evaporator to a temperature higher than 295 °C. When the solar thermal energy is 720, 960 and 1440 kW_{th}, the extraction ratio of the feed water to

the solar heat exchanger is higher than the set limit of 0.5 for keeping the feed water leaving the evaporator at a temperature lower than 295 °C, thus Method (10) becomes unfeasible. Furthermore, for a solar energy of 480 kW_{th}, Method (10) can achieve the largest solar conversion rate. This is because the feed water coming out of the evaporator, heated by solar thermal energy would operate at a higher temperature.

Flow rate of the feed water circulation was increased to15% to make it possible to heat the feed water to a high temperature by using most of the solar thermal energy without exceeding the limit on the temperature of the feed water leaving the solar heat exchanger and extraction ratio of feed water, allowing a higher solar conversion rates when the solar thermal energy increases. The model of the original CC power plant was simulated with a change of flow rate of the feed water, illustrated in Figure. 26. The net power output of the baseline CC power plant derived from this simulation was used as a new reference for estimating net power output increase after solar thermal energy integration. Meanwhile, the relation between the net power output and extraction ratio of the feed water under a new flow rate of the feed water is same with that under the original flow rate of the feed water. Figure. 27 depicts solar conversion rates for Methods (1)-(10) with the solar thermal energy ranging from 480 to 1440 kW_{th}, after the flow rate of the feed water was increased. It can be seen that Method (1) becomes unfeasible when the solar energy is 480 kW_{th}, 720 kW_{th} and 960 kW_{th} because the increasing temperature of the feed water entering the preheater makes the amount of heat recovered in the preheater much smaller. This effect leads to a decrease in CC power plant net power output. Same results were obtained for Method (2) and (5) when the solar energy input is 480 kW_{th}. Method (4) is also unfeasible under the largest level of solar thermal energy input, because at a solar energy of 1440 kW_{th}, it is difficult to keep the temperature of the water/steam leaving the superheater under the limit of 295 °C.

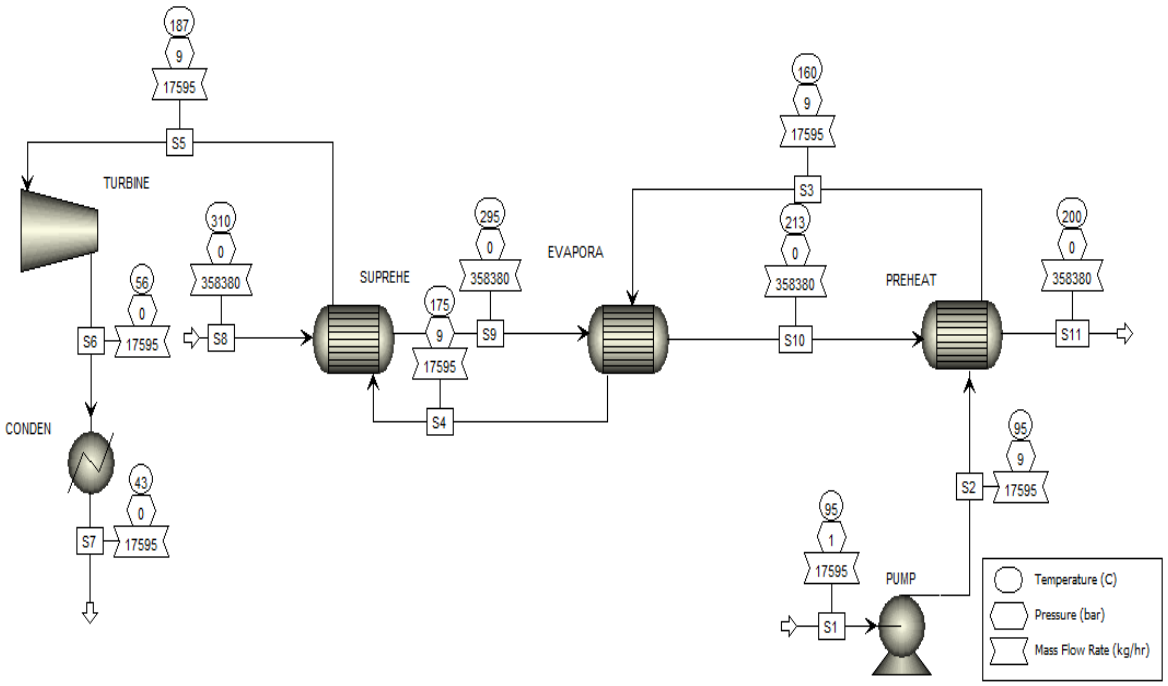

Fig. 26. Simulation diagram of the CC power plant without solar input under increased flow rate

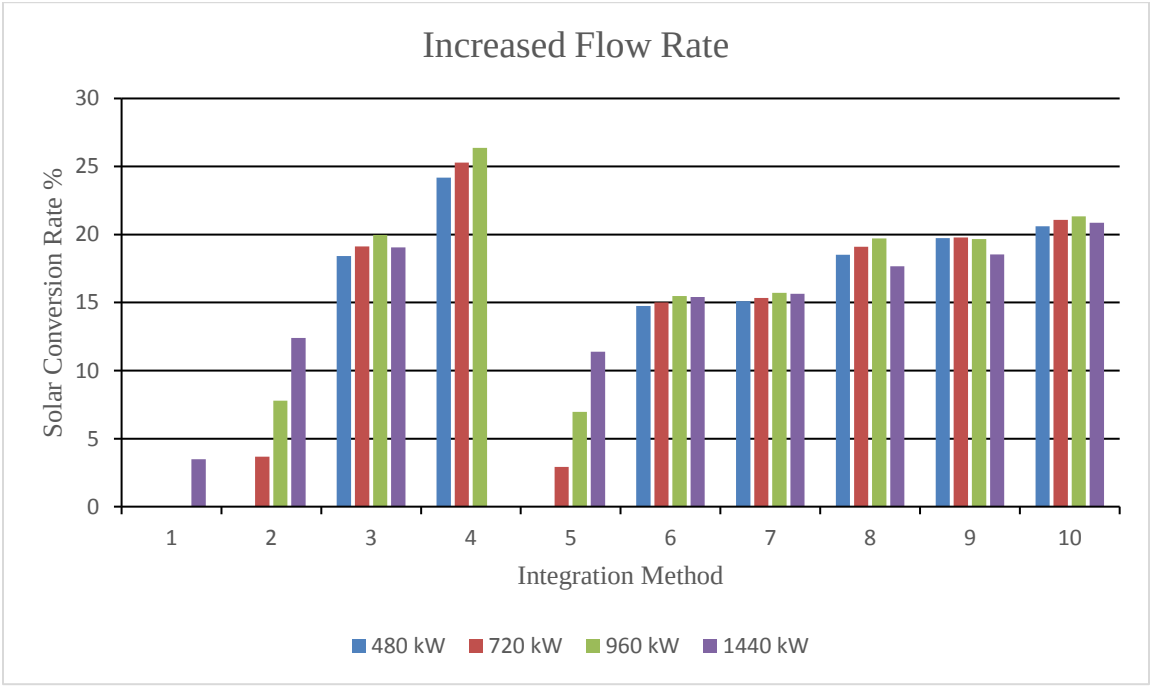

Fig. 27. Solar conversion rate of different methods with different values of solar input and increased flow rate

From Figure. 25 and Figure. 27, it can be concluded that for the same flow rate of the feed water, and irrelevant of how much solar thermal energy is used, the solar conversion rate for Method (4) is always the largest, and the solar conversion rate of Method (10) is always the second largest. The solar conversion rate of Method (3) or (9) is always the third largest. This can explain how the largest solar conversion ratio varies with the level of solar input under different flow rates of the feed water, as shown in Figures. 28-29. For original flow rate, the solar input of 480 kW_{th} has the highest solar conversion rate for the reason that the Method (10) is utilized for solar thermal energy of 480 kW_{th}, and Method (3) or (9) is utilized for solar thermal energy of 720 kW_{th}, 960 kW_{th} and 1440 kW_{th}.

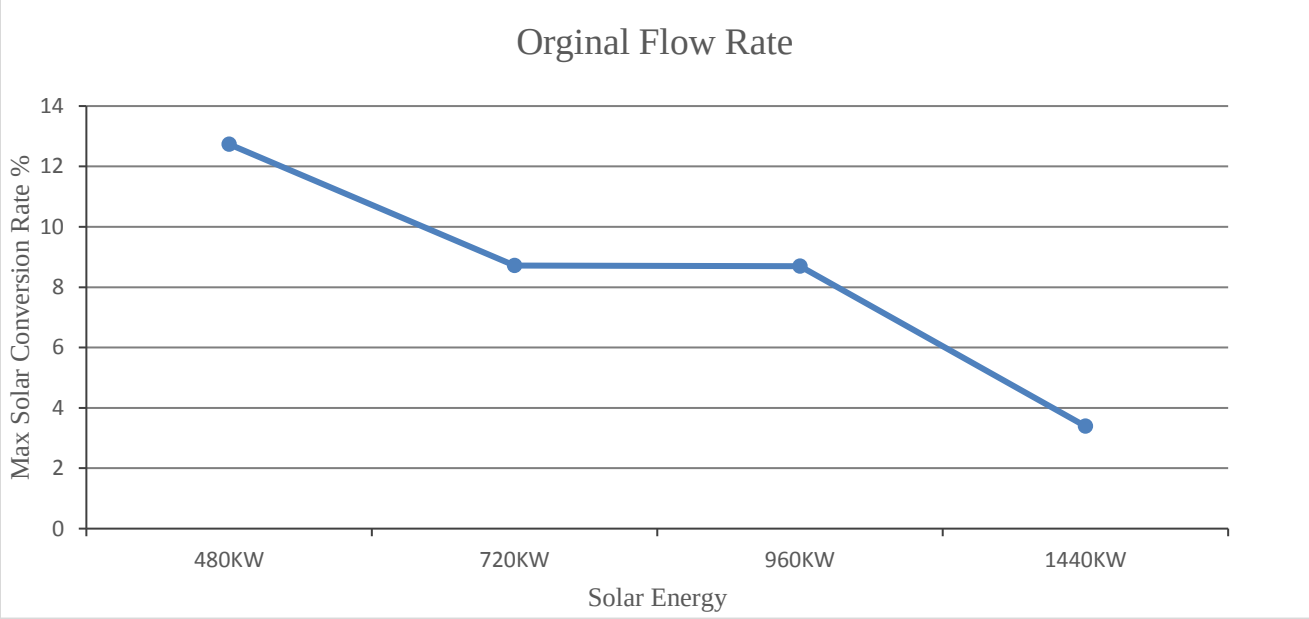

Fig. 28. largest solar conversion rates variation as a function of solar input at original flow rate

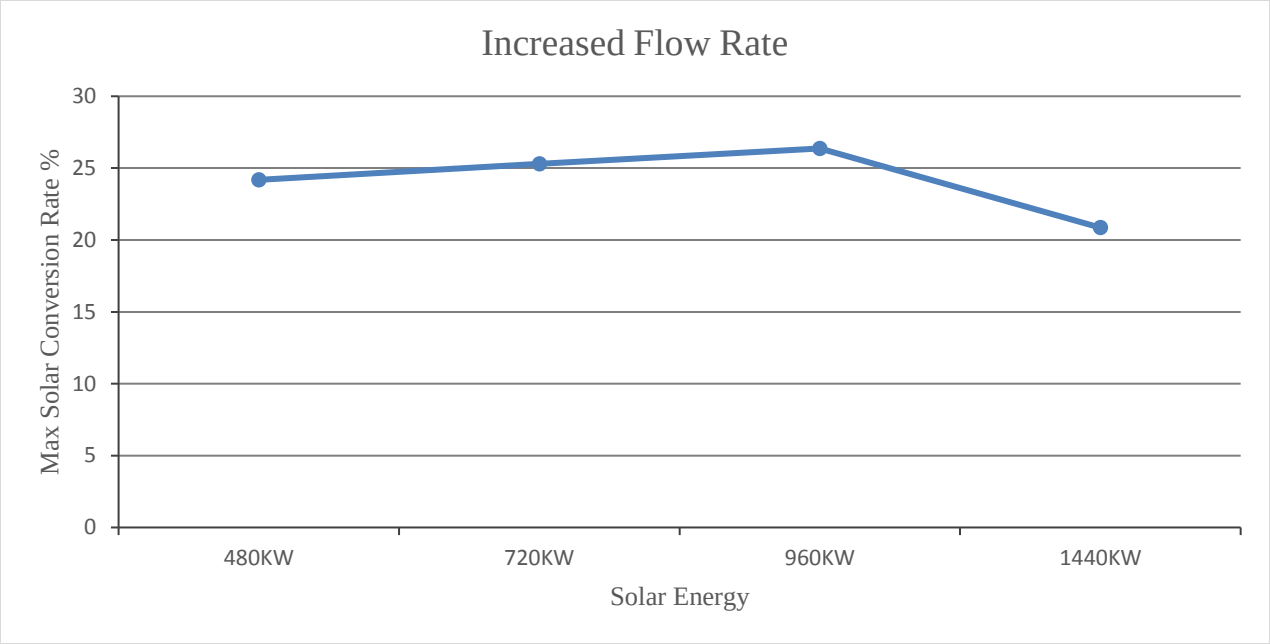

Fig. 29. Largest solar conversion rates variation as a function of solar input at increased flow rate

For the increased flow rate of the feed water, the solar conversion rate which is achieved by Method (4) for solar input of 480, 720 and 960 kW_{th} is larger than that achieved through Method (10) for the solar input of 1440 kW_{th}. Figure. 30 depicts the largest solar conversion rate achieved by all methods for each level of solar thermal energy input under different flow rates of the feed water. It shows how the largest solar conversion rate varies with the flow rate of the feed water. For a solar energy of 480 kW_{th}, the largest solar conversion rate increases for the reason that the method of integration switches from (10) to (4) after the flow rate of feed water is increased. When the solar input is 720 kW_{th}, the largest solar conversion rate gets higher because the method of integration switches from (8) to (4) under an increased flow rate of the feed water, which also happens when the solar input is 960 kW_{th}. Besides, an increase of the flow rate of the feed water makes it possible for Method (9) to be used when the solar input is 1440 kW_{th}, and the biggest solar conversion rate becomes higher.

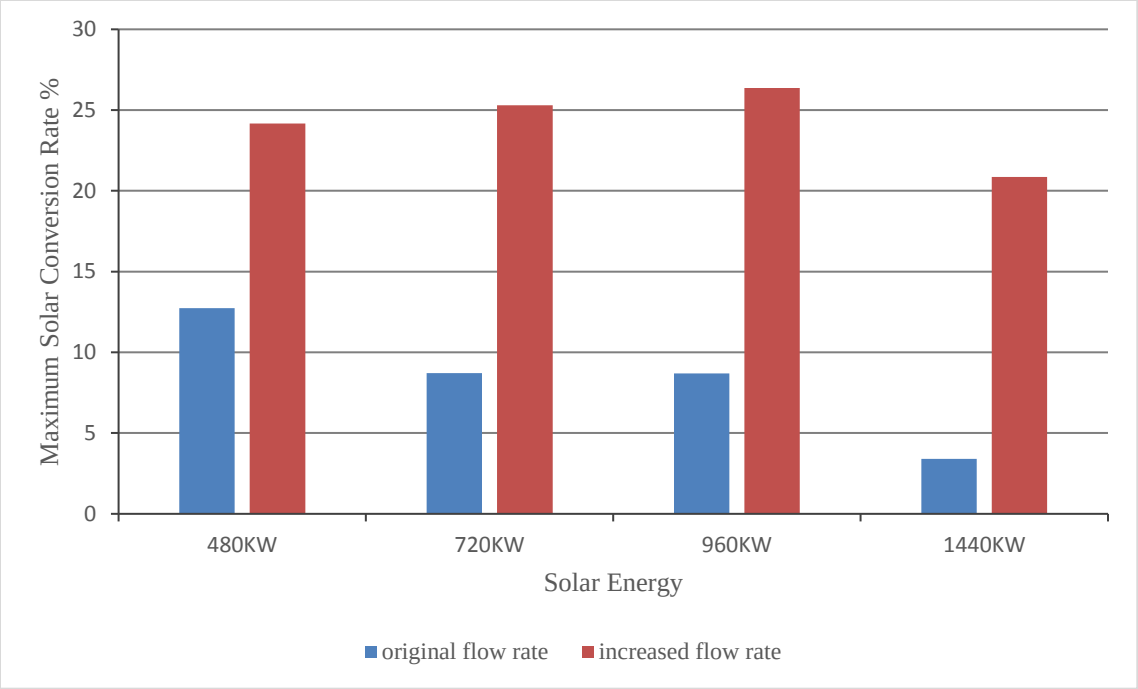

Fig. 30. Largest solar conversion rates vs the flow rate for different solar input

CHAPTER 5: Conclusions and Recommendations

In this study, complete simulations were performed for different approaches of integrating a HRSG of a CC power plant with solar thermal energy, in order to find the largest solar conversion rate. The power plant studied in this paper is located in Mexico, which is a place with great solar resources. Two different options of the integration were proposed and illustrated in process diagrams, which can be categorized into heating all feed water in the circulation loop of the steam cycle or heating the feed water extracted from the circulation loop and adding it back to the cycle. Option 1 has different locations to heat feed water, and Option 2 has different locations to extract the feed water as well as different locations to return the feed water after solar heating. Simulations of the CC power plant were conducted in ASPEN Plus based on the design data of the original CC power plant. Then models of the different integration options are built in ASPEN Plus based on the technical data of all process units of the original CC power plant without solar input. The solar conversion rates of different methods with different values of solar thermal energy, under different flow rates of the feed water were presented and compared. Based on the assumptions taken for the simulations, several methods were deemed unfeasible for the reason that the temperature of the feed water leaving the solar heat exchanger or the extraction ratio of the feed water to the solar heat exchanger exceeds practical plant limits. The following conclusions are drawn from this study:

(a) For methods included in Option 2, which includes heating feed water extracted from the circulation loop, the solar conversion rate decreases with increasing extraction ratio of the feed water. In the meantime, increasing the extraction ratio of the feed water can lead to a higher temperature of the feed water leaving the solar heat exchanger. The extraction ratio of the feed water which corresponds to the upper temperature limit, 295 °C can generate the maximum solar conversion rates for each method included in Option 2.

(b) Regardless of the values of solar energy input and flow rates of the feed water, heating the feed water leaving the superheater is always the best method to generate the largest solar conversion rate possible. Heating the feed water extracted from the point after the evaporator and adding it back to the point after the superheater can generate the second largest solar conversion rate possible. However, when these two methods are used, the temperature of the feed water leaving the solar heat exchanger or the extraction ratio of the feed water to the solar heat exchanger can easily exceed the imposed constraints

(c) The flow rate of feed water circulation can be increased to lower the temperature of the feed water leaving solar heat exchanger and the extraction ratio of the feed water, which makes it feasible to utilize method (4) and (10) under certain values of solar thermal energy without exceeding the limits.

There are still some areas which need to be investigated in future studies:

(a) An exergy analysis of the integration could help quantify the benefits of different temperature distribution of the feed water under each integration method. This investigation would provide a better handle into the relation between solar conversion rate and exergy of the feed water can be revealed.

(b) Solar conversion rates under different load of the diesel engine were not investigated. The properties of the flue gas leaving the diesel engine which include flue gas temperature, compositins and pressure change which change with the load of the diesel engine. Integrating solar energy under different diesel engine load based on daily load profiles would provide a better picture of the ultimate benefit for solar energy integration.

(c) In this study, the benefit of solar integration was investigated based on the first law of thermodynamics. An economic analysis of the entire thermal power plant after solar energy input,

LCOE and operational cost increase of using solar energy is needed. Thus, the comparison of different approaches of integration can be made more comprehensive for policy makers and investors.

REFERENCES

[1] N.L. Panwar, S.C. Kaushik, Surendra Kothari, Role of renewable energy sources in environmental protection: A review, Renewable and Sustainable Energy Reviews 15 (2011) 1513-1524.

[2] Soteris A. Kalogirou, Solar thermal collectors and applications, Progress in Energy and Combustion Science 30 (2004) 231-295.

[3] Dincer I, Rosen MA, A worldwide perspective on energy, environment and sustainable development, Int J Energy Res. 22 (15) (1998) 1305-21.

[4] Colonbo U, Development and the global environment, In: Hollander JM, editor, The energy-environment connection, Washington: Island Press, 3-14.

[5] Bergmann A, Colombo S, Hanley N, Rural versus urban preferences for renewable energy developments, Ecological Economics 44 (3) (2008) 218-23.

[6] Zakhidov RA, Central Asian countries energy system and role of renewable energy sources, Applied Solar Energy 44 (3) (2008) 218-23.

[7] Rathore NS, Panwar NL, Renewable energy sources for sustainable development, New Delhi, India: New India Publishing Agency (2007).

[8] S. Mekhilef, R. Saidur, A. Safari, A review on solar energy use in industries, Renewable and Sustainable Energy Reviews 15 (2011) 1777-1790.

[9] Nandwani SS, Solar cookers cheap technology with high ecological benefits, Ecological Economics 17 (1996) 73-81.

[10] Kalogirou S, The potential of solar industrial process heat applications, Applied Energy 76 (December (4)) 337-61.

[11] Woojoo Han, Youngjae Lee, Jihoon Jang, Kang Y. Huh, Simulation of Flow field and Carbon Monoxide Emission in an Industrial Scale Heat Recovery Steam Generator, Applied Thermal Engineering (2017).

[12] Nezammahalleh H, Farhadi F, Tanhaemami M, Conceptual design and techno-economic assessment of Integrated Solar Combined Cycle System with DSG technology, Sol. Energy 84 (2010) 1696-705.

[13] Li Yuanyuan, Yang Yongping, Thermodynamic analysis of a novel integrated solar combined cycle, Appl. Energy 122 (2014) 133-42.

[14] Behar O, Kellaf A, Mohamedi K, Ait-Kaci S, A review of Integrated Solar Combined Cycle System (ISCC) with a parabolic trough technology, Renew. Sustain Energy Rev 39 (2013) 223-50.

[15] Peterseim J, White S, Tadros A, Hellwing U, Concentrated solar power hybrid plants, which technologies are best suited for hybridization? Renew. Energy 57 (2013) 520-32.

[16] EI-Sayed MAH, Solar supported steam production for power generation in Egypt, Energy Pol 33 (2005) 1251-9.

[17] Behar O, Kellaf A, Mohamedi K, Belhamel M, Instantaneous performance of the first integrated solar combined cycle system in Algeria Energy Proc 6 (2011) 185-93.

[18] Mannuel Romero, Aldo Steinfeld, Concentrating solar thermal power and thermochemical fuels, Energy & Environmental Science (2012).

[19] Kelly B, Herrmann U, Hale MJ, Optimization studies for integrated solar combined cycle systems, In Proceedings of solar forum 2001 solar energy: the power to choose, Washington (DC). 21-25, 2001.

[20] Rovira A, Montes MJ, Varela F, Gil M, Comparison of heat transfer fluid and direct steam generation technologies for integrated solar combined cycles, Appl. Therm. Eng. 52 (2013) 264-74.

[21] Mokheimer Esmail MA, Dabwan Yousef N, Habib Mohamed A, Said Syed AM, Al-Sulaiman Fahad A, Development and assessment of integrating parabolic trough collectors with steam generation side of gas turbine cogeneration systems in Saudi Arabia, Applied Energy 141 (2015) 131-42.

[22] M.J. Montes, A. Rovira, M. Munoz, J.M. Martinez-Val, Performance analysis of an Integrated Solar Combined Cycle using Direct Steam Generation in parabolic trough collectors, Applied Energy 88 (2011) 3228-3238.

[23] Jürgen Dersch, Michael Geyer, Ulf Herrmann, Scott A. Jones, Bruce Kelly, Rainer Kistner, Winfried Ortmanns, Robert Pitz-Paal, Henry Price, Trough integration into power plants-a study on the performance and economy of integrated solar combined cycle systems, Energy 29 (2004) 947-959.

[24] M. T. Mabrouk, A. Kheiri, M. Feidt, A systematic procedure to optimize Integrated Solar Combined Cycle powr plants (ISCCs), Applied Thermal Engineering 136 (2018) 97-107.

[25] Philip G. Brodrick, Adam R. Brandt, Louis J. Durlofsky, Operational Optimization of an integrated solar combined cycle under practical time-dependent constraints, Energy 15 (2017) 1569-1584.

[26] A. Baghernejad, M. Yaghoubi, Exergoeconomic analysis and optimization of an Integrated Solar Combined Cycle System (ISCC) using genetic algorithm, Energy Conversion and Management 52 (2011) 2193-2203.

[27] Moore Jared, Apt Jay, Can hybrid solar-fossil power plants mitigate CO_2 at lower cost than PV or CSP? Environ. Sci. Technol. 47 (2013) 2487-93.

[28] Bander Jubran Alqahtani, Dalia Patiño-Echeverri, Integrated Solar Combined Cycle Power Plants: Paving the way for thermal solar, Applied Energy 169 (2016) 927-936.

[29] Mechthild Horn, Heiner Führing, Jürgen Rheinländer, Economic analysis of integrated solar combined cycle power plants. A sample case: The economic feasibility of an ISCCS power plant in Egypt, Energy 29 (2004) 935-945.

[30] R. Hosseini, M. Soltani, G. Valizadeh, Technical and economic assessment of the integrated solar combined cycle power plants in Iran, Renewable Energy 30 (2004) 1541-1555.

[31] Eduardo José Cidade Cavalcanti, Exergoeconomic and exergoenvironmental analyses of an integrated solar combine cycle system, Renewable and Sustainable Energy Reviews 67 (2017) 507-519.

[32] Sairam Adibhatla, S.C. Kaushik, Energy, exergy and economic (3E) analysis of integrated solar direct steam generation combined cycle power plant, Sustainable Energy Technologies and Assessments 20 (2017) 88-97.

[33] Esmail .M.A. Mokeheimer, Yousef N. Dabwan, Mohamed A. Habib, Optimal integration of solar energy with fossil fuel gas turbine cogeneration plants using three different CSP technologies in Saudi Arabia, Applied Energy 185 (2017) 1268-1280.

[34] Fogler & Gurmen, Aspen Plus™ INFORMATION. University of Michigan (2007).

[35] Department of Energy, https://www.energy.gov/energysaver/solar-water-heaters/heat-transfer-fluids-solar-water-heating-systems.

VITA

Tianjun Han was born on January 4th, 1994 in Wuhan, son of Yalong Tian and Chunsheng Han. He attended Wuhan University in September 2012 after graduating from the No.1 Middle School Attached to Central China Normal University. In July 2014, he went to University of California, Berkeley for summer school. In July 2015, he had an internship in GE Wuhan Boiler Co., Ltd as an assistant to the LEAN department. He graduated from Wuhan University with a bachelor degree of engineering in energy dynamics system and its automation, in June 2016. In September 2016, he started at Lehigh University. Now, he is a graduate student in the Department of Mechanical Engineering at Lehigh University.